https://doi.org/10.5194/egusphere-2025-4179
Preprint. Discussion started: 23 September 2025

Unravelling groundwater's role in soil-plant-atmosphere continuum: Integrated ecohydrological modelling approach using STEMMUS-SCOPE and MODFLOW 6

Mostafa Gomaa Daoud[1], Fakhereh (Sarah) Alidoost[2], Yijian Zeng[1], Bart Schilperoort[2], Christiaan Van der Tol[1], Maciek W. Lubczynski[1,3], Mhd Suhyb Salama[1], Eric D. Morway[4], Christian D. Langevin[5], Prajwal Khanal[1], Zengjing Song[1], Lianyu Yu[6,7], Hong Zhao[8], Gualbert Oude Essink[9,10], Victor F. Bense[11], Michiel van der Molen[8], Zhongbo Su[1]

[1] Department of Water Resources, Faculty of Geo-Information Science and Earth Observation (ITC), University of Twente, PO Box 217, 7522 NH Enschede, The Netherlands

[2] Netherlands eScience Center, Amsterdam, 1098XH, the Netherlands

[3] Civil Engineering School & Department, University of A Coruña, Campus Elviña s/n, 15071 A Coruña, Spain

[4] U.S. Geological Survey, Nevada Water Science Center, Carson City, NV, USA

[5] S.S. Papadopulos & Assoc., Inc., 12 Dove Lane, Saint Paul, MN, USA

[6] College of Water Resources and Architectural Engineering, Northwest Agriculture and Forestry University, Yangling, China

[7] Key Laboratory of Agricultural Soil and Water Engineering in Arid Area of Ministry of Education, Northwest Agriculture and Forestry University, Yangling, China

[8] Meteorology and Air Quality Section, Wageningen University and Research, Wageningen, The Netherlands

[9] Unit Subsurface and Groundwater Systems, Deltares, P.O. Box 85467, 3508 AL, Utrecht, The Netherlands

https://doi.org/10.5194/egusphere-2025-4179
Preprint. Discussion started: 23 September 2025

[10] Department of Physical Geography, Utrecht University, PO Box 80125, 3508 TC Utrecht, The Netherlands

[11] Department of Environmental Sciences, Wageningen University and Research, Wageningen, The Netherlands

Corresponding author: Mostafa Gomaa Daoud (m.g.m.daoud@utwente.nl)

Abstract

Soil-plant-atmosphere continuum (SPAC) models are commonly used to investigate various components' role(s) in ecosystem functioning. Yet, in most SPAC models, groundwater is ignored or at best represented in an over-simplified manner, leading to misunderstanding of its critical role in simulating soil-vegetation dynamics. This study investigates the groundwater's role in soil-plant-atmosphere processes. To this end, an integrated ecohydrological modelling (IEM) framework is developed by coupling the STEMMUS-SCOPE SPAC model to the MODFLOW 6 integrated hydrological model. The standalone STEMMUS-SCOPE (ST-SC) and coupled STEMMUS-SCOPE-MODFLOW 6 (ST-SC-MF6) models were applied over an 8-year period (1 April 2016 – 31 March 2024) to three sites in the Netherlands (Loobos, Cabauw and Veenkampen). Simulated various essential variables, including soil moisture (θ), soil temperature (T_s), groundwater level, groundwater temperature, evapotranspiration (ET), gross primary productivity, net ecosystem exchange (NEE), and sun-induced chlorophyll fluorescence (SIF) were then compared to corresponding in-situ observations to evaluate the ST-SC and ST-SC-MF6 setups. Results indicated that the groundwater contribution is spatially and temporally variable. ST-SC-MF6 showed better agreement with observations than ST-SC for: a) T_s, and ET at Loobos, b) θ, ET, NEE, and SIF at Cabauw, and c) θ, and ET at Veenkampen. Notably, benefits of ST-SC-MF6 simulation were particularly prominent during dry periods, when shallow groundwater mitigated vegetative water stress. Overall, the proposed ST-SC-MF6 IEM helped to: (1) incorporate groundwater as a key component in the water, energy and

https://doi.org/10.5194/egusphere-2025-4179
Preprint. Discussion started: 23 September 2025

carbon cycles, and (2) define the important role groundwater dynamics play in soil-plant-atmosphere continuum for deepening our understanding of ecosystem functioning.

Short summary

This study investigates the groundwater role in soil-plant-atmosphere continuum. An integrated ecohydrological modelling approach was developed by coupling STEMMUS-SCOPE to MODFLOW 6 and applied at three sites over 8 years. The coupled model improved simulations of soil moisture and temperature, evapotranspiration, carbon fluxes and fluorescence. The findings highlight the groundwater critical role in ecosystem dynamics and its contribution to advancing water, energy and carbon cycle modelling.

1. Introduction

The interactions among the soil, water, vegetation and atmosphere play a fundamental role in regulating ecosystem functioning. These interactions include hydrological, thermal and carbon processes that collectively shape the dynamics of the water, energy and carbon cycles. Deepening our understanding of such interactions is crucial for better supporting ecosystem resilience against the adverse impact of climate change and anthropogenic activities (Chen et al., 2024; Dai et al., 2024). Essential climate variables (ECVs) are globally recognized indicators that characterize the Earth's system (Bojinski et al., 2014; GCOS, 2025). Terrestrial ECVs include key indicators of vegetation status such as leaf area index, above-ground biomass, and fraction of absorbed photosynthetically active radiation. Recent studies (Baatz et al., 2021; Cupertino et al., 2024; Muise et al., 2024) have expanded beyond the traditional ECVs to include: a) productivity variables — including gross primary productivity, net ecosystem exchange, and evapotranspiration (Baatz et al., 2021); b) structure variables — including canopy height, canopy cover, and below-ground biomass (Atkins et al., 2018; de Conto et al., 2024); and c) development variables — including plant phenology (start and end of growing season; Shi et al., 2023) and more recently the sun-induced chlorophyll fluorescence (SIF), which serves as a proxy for tracking the photosynthesis process (Sun et al., 2023). Additionally, other soil-related variables play a significant role in characterizing the ecosystems' functioning, such as soil moisture, surface and subsurface temperature, and evaporation (Bojinski et al., 2014; Zeng et al., 2019; GCOS, 2025).

Soil-plant-atmosphere continuum (SPAC) models are widely used to simulate most of the aforementioned ECVs. SPAC models simulate the transfer of thermal energy and mass (water and carbon) between soils, plants (through roots, stems and leaves), and the atmosphere (Guo, 1992). Furthermore, SPAC models are capable of assimilating remote sensing information such as canopy reflectance, vegetation optical depth, and SIF (Yang et al., 2021). Integrating the RS data into SPAC models enables upscaling the processes from point (plant) scale to regional scales (Senf, 2022; Van Cleemput et al., 2025), allowing for predicting ecosystem responses to regional environmental changes (Dronova & Taddeo, 2022). Examples of SPAC models are the Community Land Surface (CLM5) model (Lawrence et al., 2019), the STEMMUS-SCOPE model (Wang et al., 2021), the Tethys-Chloris (T&C) model (Fatichi et al., 2012), the Soil-Plant-Atmosphere (SPA) model (Williams et al., 1996; Williams et al., 2001), and the SWAP model [(van Dam et al., 2008) – specifically the version coupled to the WOFOST model (de Wit et al., 2019)]. However, SPAC models either ignore or oversimplify the underlying groundwater system by neglecting spatio-temporal variability in groundwater variables (e.g., head and temperature), and processes (e.g., recharge, discharge and groundwater evapotranspiration). Thus, the SPAC models lack or simplify the groundwater influence on the simulated soil-plant-atmosphere processes.

For most landscapes, groundwater storage is generally the largest component of the local water budget. It plays a vital role in sustaining essential ecosystem services by mitigating biodiversity loss and buffering against climate change (Saccò et al., 2024). Many ecosystems rely primarily on groundwater resources, so-called groundwater-dependent ecosystems, to maintain their ecological functions (Kløve et al., 2014). Groundwater-dependent ecosystems can be exposed to surface water – groundwater interactions, which enhance groundwater discharge and likely face significant impairment under future climate regimes (Otoo et al., 2025). Groundwater can also have a significant effect in enhancing carbon assimilation, plant growth and productivity (Ruehr et al., 2023). Under shallow water table conditions, the groundwater dynamics are significant, exerting a strong influence on the soil moisture distribution and the evapotranspiration rates (Martínez-De La Torre & Miguez-Macho, 2019). Additionally, groundwater processes operate at a slower pace, as compared to surface water systems or the soil zone, leading to latency in their responses to environmental changes, such as drought. This delayed response allows the groundwater to support vegetation in mitigating water stress effects during prolonged drought periods. Marchionni et al. (2020) demonstrated that the presence of the water table within the vegetation rooting depth supported the ecosystem transpiration and vegetation productivity during a prolonged drought event (2001-2009) near Melbourne, Australia.

Groundwater and its interaction with the surface (through the unsaturated zone) are often simulated by integrated hydrological models (IHMs). IHMs simulate flow processes in the surface and subsurface domains, including their dynamic interaction (i.e., flow exchange) within a single simulation environment (Daoud et al., 2022; 2024). IHMs are used for assessing water resources and evaluating future scenarios for sustainable water resources management (Lubczynski et al., 2024). Examples of IHMs are Hydrogeosphere (Brunner & Simmons, 2012), MIKE SHE (Graham & Butts, 2005), CATHY (Camporese et al., 2010), and MODFLOW 6 (Langevin et al., 2017; Langevin et al., 2023). However, IHMs, by themselves, do not consider ecosystem functioning in terms of explicitly simulating the carbon cycle or detailed plant processes. Consequently, IHMs are not often used to evaluate ecosystem functioning and the interactions between the water, energy and carbon cycles.

Despite the critical role groundwater plays in sustaining many different types of ecosystems, SPAC models, unlike IHMs, typically lack a physically-based groundwater model. Instead, SPAC models

https://doi.org/10.5194/egusphere-2025-4179
Preprint. Discussion started: 23 September 2025

commonly assume that soil moisture dynamics are primarily driven by infiltration (generated from precipitation or applied irrigation) and either ignore or oversimplify groundwater and its connection to the soil and the vegetation domains (Samuel & Chakraborty, 2023). Notably, SPAC models typically do not account for heterogeneity in any of the aquifer properties (porous media or fractured-rock systems), which can be significant in shaping key groundwater processes such as recharge, capillary rise, and groundwater evapotranspiration (Ireson et al., 2013; Xin et al., 2023). Thus, SPAC models are not equipped to accurately capture the effect of salient groundwater processes while simulating soil and vegetation dynamics. Additionally, SPAC models ignore or simplify spatio-temporal groundwater temperature dynamics. However, many recent studies (Xin et al., 2023; Benz et al., 2024; Egidio et al., 2024; Rammler & Bertermann, 2025) showed that soil temperatures are modulated not only by surface-atmosphere heat exchange processes, but also by soil zone-groundwater heat exchange processes (i.e. conductive and advective heat transport), especially in cases of shallow water table conditions. Ignoring the thermal dynamics of groundwater can subsequently lead to biases in simulating soil temperature, which is a key driver for photosynthesis, evapotranspiration (specifically latent heat flux), and carbon fluxes. Omitting or simplifying the groundwater component (for flow and heat processes) in SPAC models may also lead to misrepresentation of soil and plant physiological responses to changing ambient (climatic) conditions; thereby limiting the usefulness of SPAC models for appraising the impact of a changing climate on groundwater-dependent ecosystems (Elrashidy et al., 2023) or, more generally, ecosystems with shallow groundwater conditions.

Given the limitations of both the SPAC models and IHMs, an integrated modelling approach, that combines hydrology with ecosystem functioning, would result in a modeling tool that is better suited for evaluating ecosystem functioning under a changing climate. An integrated SPAC-IHM model is hereafter referred to as an integrated ecohydrological model (IEM). The advantage of an IEM is that it can simulate the full continuum of water (including groundwater), energy, and carbon fluxes at high temporal resolution within a single simulation environment. IEMs are also capable of

https://doi.org/10.5194/egusphere-2025-4179
Preprint. Discussion started: 23 September 2025

integrating the subsurface hydrology (both unsaturated and saturated zones) with plant physiological processes, as well as incorporating remote-sensing information (as inputs) for simultaneous simulation of multiple variables [i.e., soil moisture (θ), soil temperature (T_s), evapotranspiration (ET), gross primary productivity (GPP), SIF, groundwater level (GWL), and groundwater temperature (GT)] that are vital for accurately characterizing ecosystem dynamics. Furthermore, IEMs facilitate the simulation of continuous moisture and temperature profiles from the subsurface to the top of the canopy. Table 1 lists the few existing IEMs that can physically simulate energy, carbon and water processes, including groundwater flow. The list include the enhanced CLM5 (Akhter et al., 2025), the Terrestrial System Modeling Platform (TSMP, Shrestha et al., 2014; Gasper et al., 2014), the enhanced version (Liao et al., 2025) of the Earth system model (E3SM; Golaz et al., 2022) and the MODFLOW-MetaSWAP–WOFOST (Van Walsum & Supit, 2012). While all these IEMs can simulate the water processes, including detailed groundwater flow processes, they all lack the representation of groundwater heat processes and groundwater temperature simulation. Furthermore, none of them account for SIF simulation. Hence, a new IEM is needed that can physically-based integrate the groundwater processes (mass and energy) with detailed energy, carbon and SIF fluxes. The hypothesis of this study is that explicit representation of groundwater mass and energy in an IEM framework improves quantification of the soil–plant–atmosphere continuum and deepens our understanding of ecosystem functioning.

https://doi.org/10.5194/egusphere-2025-4179
Preprint. Discussion started: 23 September 2025

163 Table 1. List of available integrated ecohydrological models (IEMs)

Model name	Water cycle processes			Heat transfer processes		Energy cycle, ET and root growth & uptake	Carbon cycle and photosynthesis	SIF	Reference
	Surface water (runoff and streamflow)	Unsaturated zone flow	Groundwater flow	Unsaturated zone	Groundwater zone				
Enhanced CLM5	Yes	Yes, 1D Richards equation	Yes, by incorporating an aquifer beneath the soil column to allow for lateral groundwater flow and pumping	Yes	No	Yes	Yes	No	(Akhter et al., 2025)
TSMP (COSMO-CLM3.5-ParFlow)	Yes	Yes, via ParFlow (3D Richards equation)	Yes, via ParFlow (3D Richards equation)	Yes	No	Yes	Yes	No	(Shrestha et al., 2014; Gasper et al., 2014)
Enhanced E3SM	Yes	Yes	Yes, by developing a new hillslope-based hydrological model to simulate lateral groundwater flow	Yes	No	Yes	Yes	No	(Liao et al., 2025)
MODFLOW-MetaSWAP–WOFOST	Yes	Yes, 1D Richards equation	Yes, via MODFLOW (1D/2D/3D).	Yes	No	Yes	Yes, via WOFOST	No	(Van Walsum & Supit, 2012)
STEMMUS–SCOPE–MODFLOW 6	Yes	Yes, 1D Richards equation	Yes, via MODFLOW 6 (1D/2D/3D). 1D is used in this study	Yes	Yes, via MODFLOW 6	Yes	Yes	Yes	This study

164

This study aims to investigate the role of groundwater in the soil-plant-atmosphere continuum with a focus on assessing the benefits of explicitly incorporating the groundwater component in modelling soil-plant-atmosphere processes. To this end, a new IEM framework is developed by tightly coupling the STEMMUS-SCOPE SPAC model to the MODFLOW 6 IHM model. The STEMMUS-SCOPE-MODFLOW 6 is tested in a 1-dimensional (1D) setup (which will be extended to 2D/3D in a follow up study) applied to three sites in the Netherlands (i.e., Loobos, Cabauw, and Veenkampen). Simulated variables of interest are evaluated with and without the coupling to quantify the effect of explicitly representing groundwater within the simulation.

STEMMUS-SCOPE model (Wang et al., 2021) is a SPAC model, which is an integrated version of two separate models (STEMMUS and SCOPE). STEMMUS (Simultaneous Transfer of Energy, Mass, and Momentum in Unsaturated Soil) simulates the transfer of energy, mass, and momentum in the unsaturated zone (Zeng et al., 2011a; b; Zeng & Su, 2013). SCOPE (Soil Canopy Observation, Photochemistry, and Energy Fluxes) simulates the radiative transfer in the soil, leaves, and vegetation canopies, as well as photosynthesis and non-radiative energy dissipation through convection and mechanical turbulence (Van Der Tol et al., 2009; Yang et al., 2021). The coupling between STEMMUS and SCOPE enables the seamless soil-plant-atmosphere modelling of energy, water and carbon exchanges. Additionally, STEMMUS-SCOPE allows for simulating the influence of θ and T_s variability on vegetation dynamics in terms of photosynthesis, stomatal behavior and plant water stress responses (Tang et al., 2024). More details about the STEMMUS-SCOPE coupling are described in Wang et al. (2021).

MODFLOW 6 is an IHM framework (Hughes et al., 2017) and is the latest “core” version of the well-known MODFLOW simulator for groundwater flow (GWF). In addition, MODFLOW 6 simulates other flow and transport processes, including unsaturated zone flow, overland flow, flow in surface features (e.g. lakes, rivers, drains, etc), and their interaction with the groundwater system (Langevin et al., 2017; Langevin et al., 2023). Recently, a new Groundwater Energy Transport (GWE) module,

https://doi.org/10.5194/egusphere-2025-4179
Preprint. Discussion started: 23 September 2025

patterned after the solute transport module (Langevin et al., 2022), was added to MODFLOW 6 for simulating heat transport processes within a MODFLOW 6 simulation (Morway et al., 2025) and is leveraged in this study.

2. Methods

2.1. STEMMUS-SCOPE & MODFLOW 6 coupling

The Basic Model Interface (BMI; Peckham et al., 2013; Hutton et al., 2020) is adopted as the convention for coupling STEMMUS-SCOPE to MODFLOW 6. The BMI protocol is general; models that support it can be controlled, and their variables can be accessed and set during runtime by an external program or script. BMI protocols are used for this effort to facilitate the exchange of model-calculated variables and other information between the coupled models by passing values externally; thereby eliminating the need to access (or modify) the source code(s) of the coupled models during the simulations.

2.1.1. BMI phases

BMI routines are commonly organized into three phases (initialize, update, finalize) as described in figure 2 of Hughes et al. (2022). Figure 1 shows the coupling framework of STEMMUS-SCOPE-MODFLOW 6.

<u>Initialize phase</u>

The initialization phase in a BMI setup is separate from the initialization routines associated with each of the individual models (explained in section 2.5.2). During the BMI initialization routine, "hooks" are established between the coupled models to facilitate the exchange of calculated values during a forward run. During the initialize phase, initialized head (i.e., GWL) and temperature (i.e., GT) of the water table are defined in STEMMUS-SCOPE. While, initialized groundwater net recharge

https://doi.org/10.5194/egusphere-2025-4179
Preprint. Discussion started: 23 September 2025

flux (R_n), heat flux above water table (Q_{heat}), and recharge temperature (RT_g) are defined in MODFLOW 6.

Update phase

The update phase is at the core of the coupling process (Fig. 1b). During this phase, the two models exchange variable values at the phreatic surface (the shared interface between the unsaturated zone and the saturated zone, marked by a bold blue line in the diagram of Fig. 1a). At this shared interface, STEMMUS-SCOPE requires the following bottom boundary conditions: a) specified head (i.e. GWL) for the soil water module, and b) specified temperature (i.e. GT) for the soil energy module; together to simulate groundwater gross recharge (R_g), capillary rise flux (Cap), root groundwater uptake (RWU_g), Q_{heat}, and RT_g. While MODFLOW 6 requires the following upper boundary conditions: specified water flux (i.e. R_n, calculated as the difference between R_g, Cap, and RWU_g) for the GWF module, and b) specified heat flux (i.e., Q_{heat}) and/or its specified temperature (i.e., RT_g) for the GWE module; together to simulate GWL and GT. From herein, the simulated variables (R_n, Q_{heat}, and RT_g) by STEMMUS-SCOPE are referred to as 'STEMMUS-SCOPE variables' (marked by red color in the flowchart of Fig. 1b), while the simulated variables (GWL and GT) by MODFLOW 6 are referred to as 'MODFLOW 6 variables' (marked by blue color in the flowchart of Fig. 1b).

The update phase runs in a looped manner (update loop) with number of updates equal to number of time steps. In principle, the BMI can work with different temporal discretization (number of time steps and the length of each time step) for each of the two coupled models. However, for ease of use, the same temporal discretization was used for both models in this study. For each time step: 1) MODFLOW 6 runs and updates the MODFLOW 6 variables, 2) the updated MODFLOW 6 variables are passed to STEMMUS-SCOPE (illustrated by the blue bold arrow in Fig. 1b), which are used as bottom boundary conditions by STEMMUS-SCOPE, 3) STEMMUS-SCOPE runs and updates the STEMMUS-SCOPE variables, 4) the updated STEMMUS-SCOPE variables are passed back to MODFLOW 6

https://doi.org/10.5194/egusphere-2025-4179
Preprint. Discussion started: 23 September 2025

(illustrated by the red bold arrow in Fig. 1b) to be used as upper boundary conditions for the next time step, and 5) updates continue until the last time step.

<u>Finalize phase</u>

In this phase, both models finalize their simulation, and the model outputs are exported for further analysis. The model outputs include the STEMMUS-SCOPE variables, the MODFLOW 6 variables, and other variables of interest (marked by black color in Fig. 1) as follows: θ, T_s, root soil water uptake (RWU_s), subsurface evaporation (E), ET which is the summation of E, RWU_s and RWU_g, GPP, NEE, and SIF.

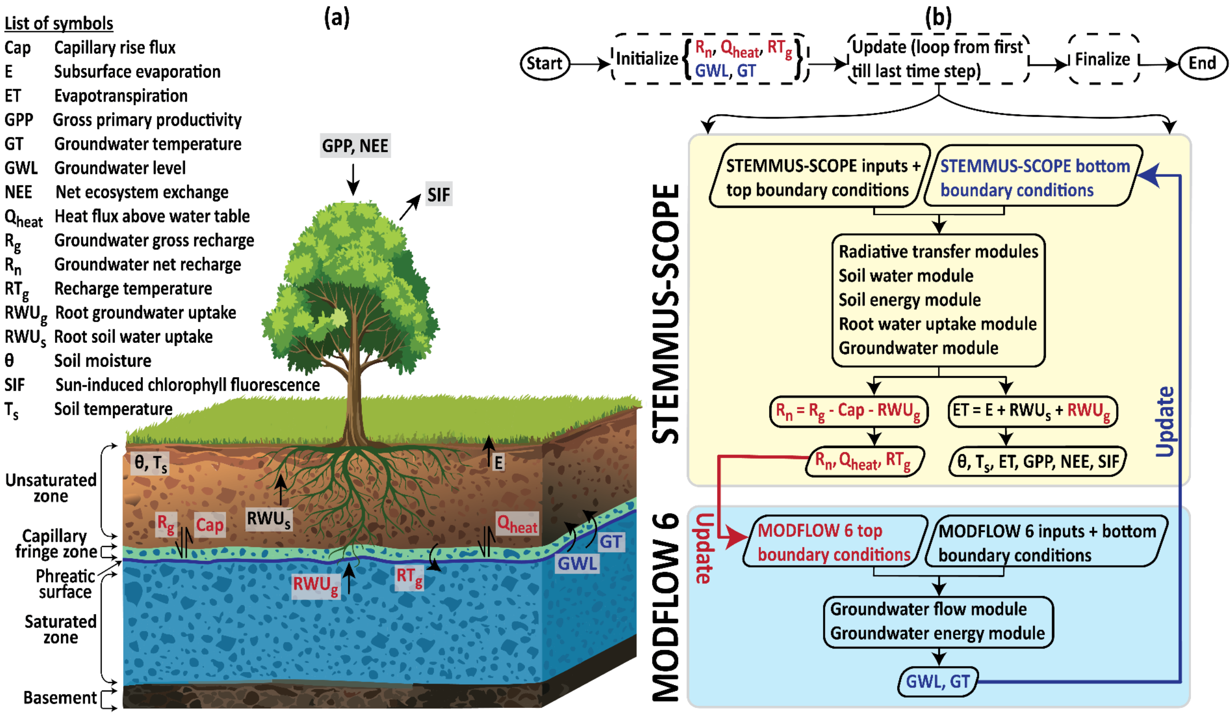

Figure 1. Schematic of the coupled STEMMUS-SCOPE and MODFLOW 6 framework: a) illustrative diagram (left panel); b) flowchart (right panel). The red color indicates the processes and/or variables that are transferred from STEMMUS-SCOPE to MODFLOW 6. The blue color indicates the processes and/or variables that are transferred from MODFLOW 6 to STEMMUS-SCOPE.

https://doi.org/10.5194/egusphere-2025-4179
Preprint. Discussion started: 23 September 2025

MODFLOW 6 was not originally written to support BMI; however, Hughes et al. (2022) documents the restructuring of the source code to align MODFLOW 6 to support the BMI conventions. Schilperoort (2025) and Zeng et al. (2025) document the steps followed to make STEMMUS-SCOPE BMI-compatible. Additionally, a groundwater module is added into the source code of STEMMUS-SCOPE to: a) recognize the effect of the saturated zone dynamics on the unsaturated zone through the MODFLOW 6 variables, and b) prepare the necessary STEMMUS-SCOPE variables that are fed into MODFLOW 6. The groundwater module includes three main parts: 1) unsaturated zone bottom boundary, 2) recharge and capillary rise flux, and 3) root groundwater uptake.

2.1.2. Unsaturated zone bottom boundary

The bottom boundary of the unsaturated zone for the soil water module in STEMMUS-SCOPE can be defined using one of three options (Zeng & Su, 2013): a) specified matric head (Dirichlet) boundary, b) specified moisture flux, and c) zero matric head (i.e. gravity drainage). For this investigation, option (a) is used. This bottom boundary (specified matric head) is adaptively positioned at the phreatic surface (Fig. 1a), corresponding to the GWL at each time step (Zeng et al., 2019). The GWL value is received by STEMMUS-SCOPE from MODFLOW 6 through the BMI (Fig. 1b). Then, at the phreatic surface elevation (GWL), the specified matric head is set to zero (matric head is negative above GWL and positive below GWL). At each time step, the GWL may rise or fall, causing the phreatic surface to shift upward or downward. As a result, the thickness of the unsaturated zone decreases or increases, and the position of the bottom boundary is updated to reflect this moving boundary condition.

Similarly, for the soil energy module, a specified temperature boundary condition is used as the bottom boundary. The value of the specified temperature is the GT (Fig. 1b), received by STEMMUS-SCOPE from MODFLOW 6 through the BMI and updated at each time step.

https://doi.org/10.5194/egusphere-2025-4179
Preprint. Discussion started: 23 September 2025

2.1.3. Recharge and capillary rise flux

STEMMUS-SCOPE simulates two-phase mass and heat flow in the unsaturated zone using the modified Richards equation (Milly, 1982). The water flow is driven by both gravity and capillary forces (Eq. 1).

$$\frac{\delta}{\delta t}(\rho_L\theta_L + \rho_v\theta_v) = \frac{-\delta}{\delta z}(q_{Lh} + q_{LT} + q_{vh} + q_{vT}) - S$$

$$= \rho_L \frac{\delta}{\delta z}\left[K\left(\frac{\delta\psi}{\delta z} + 1\right) + D_{TD}\frac{\delta T}{\delta z}\right] + \frac{\delta}{\delta z}\left[D_{vh}\frac{\delta\psi}{\delta z} + D_{vT}\frac{\delta T}{\delta z}\right] - S \quad (1)$$

where ρ_L and ρ_v (Kg m^{-3}) are the density of liquid water and water vapor, respectively; θ_L and θ_v (m^3 m^{-3}) are the soil liquid and vapor volumetric water content, respectively; q_{Lh} and q_{LT} (kg m^{-2} s^{-1}) are the soil liquid water fluxes driven by the soil matric potential gradient ($\frac{\delta\psi}{\delta z}$) and temperature gradient ($\frac{\delta T}{\delta z}$), respectively; q_{vh} and q_{vT} (Kg m^{-2} s^{-1}) are the soil water vapor fluxes driven by the $\frac{\delta\psi}{\delta z}$ gradient and the $\frac{\delta T}{\delta z}$ gradient, respectively; K is the unsaturated hydraulic conductivity (m s^{-1}); D_{TD} (Kg m^{-1} s^{-1} K^{-1}) is the transport coefficient of the adsorbed liquid flow due to temperature gradient; D_{vh} (Kg m^{-2} s^{-1}) is the isothermal vapor conductivity; D_{vT} (Kg m^{-1} s^{-1} K^{-1}) is the thermal vapor diffusion coefficient, and S is the sink term (m s^{-1}). More details of the equation are in Zeng et al. (2011a, b) and Zeng & Su (2013).

As explained in section 2.1.1, the GWL is adopted as the bottom boundary condition of the unsaturated zone in STEMMUS-SCOPE. Consequently, a capillary fringe zone is formed above the phreatic surface (Fig. 1a), where water is pulled up from the saturated zone by capillary forces. Moreover, when precipitation infiltrates into the unsaturated zone and percolates downward, it has to go through the capillary fringe zone and continue downward as R_g to the saturated zone. Hence, the capillary fringe zone includes both the R_g and the Cap. The R_g and the capillary rise flux (Cap), the latter contributes to groundwater evaporation (Balugani et al., 2017), are calculated from the summation of q_{Lh}, q_{LT}, q_{vh}, and q_{vT} fluxes (Eq. 2) at the capillary fringe zone. The result of that summation determines whether the calculated flux (Q, Eq. 2a) represents $\mathrm{R_g}$ or Cap. If the summation is negative (Eq. 2b), it means the flow direction is downward, and the $\mathrm{R_g}$ term is dominant. In contrast, if the summation is positive (Eq. 2c), it means the flow direction is upward, and the Cap term is dominant. In STEMMUS-SCOPE, upward fluxes (capillary rise) are positive, while downward fluxes (gravity drainage) are negative. However, MODFLOW 6 uses the opposite sign convention. Therefore, the $\mathrm{R_g}$/Cap is multiplied by -1, when transferred to MODFLOW 6 through the BMI.

$$\mathrm{Q = q_{Lh} + q_{LT} + q_{vh} + q_{vT}} \tag{2a}$$

$$\mathrm{R_g = Q} \qquad \text{if } Q < 0 \tag{2b}$$

$$\mathrm{Cap = Q} \qquad \text{if } Q \geq 0 \tag{2c}$$

2.1.4. Root groundwater uptake

The root water uptake (RWU) is calculated in STEMMUS-SCOPE based on a resistance scheme that takes into account the hydraulic gradient between the soil water potential (ψ_i) and the leaf water potential (ψ_l) (Eq. 3). The root water uptake module, developed by Wang et al. (2021), takes into account the θ as the only source of water for the roots (root soil water uptake, $\mathrm{RWU_s}$), meaning that RWU = $\mathrm{RWU_s}$. $\mathrm{RWU_s}$ is calculated for all the soil layers that are above the maximum rooting depth ($\mathrm{d_{max}}$).

$$\mathrm{RWU} = \sum_{i=1}^{n} \frac{\psi_{s,i} - \psi_l}{r_{s,i} + r_{r,i} + r_{x,i}} \text{ and } \mathrm{RWU_s = RWU} \tag{3}$$

where

$\psi_{s,i}$ is the soil water potential of layer i (m), ψ_l is leaf water potential (m), $r_{s,i}$ is the soil hydraulic resistance (s m^{-1}), $r_{r,i}$ is the root resistance to water flow radially across the roots (s m^{-1}), and $r_{x,i}$ is the plant's axial resistance to flow from the root xylem to the leaves (s m^{-1}).

https://doi.org/10.5194/egusphere-2025-4179
Preprint. Discussion started: 23 September 2025

However, the roots can uptake water from an additional source (root groundwater uptake, RWU_g) if the roots have access to groundwater (GWL is above d_{max}). As explained in section 2.1.1, the GWL is adopted as the bottom boundary condition of the unsaturated zone for the soil water module in STEMMUS-SCOPE, hence, the RWU is also influenced. The RWU calculations were updated by splitting it into two components (RWU_s and RWU_g, Eq. 4). The RWU_s is for the soil layers that are above the capillary fringe zone and above d_{max} (Eq. 5), and the RWU_g is for the soil layers that are below the capillary fringe zone and above d_{max} (Eq. 6). The RWU_s and RWU_g are calculated by replacing the soil water potential ($\psi_{s,i}$) in Eq. (4) with the updated $\psi_{s,i}$ (due to the effect of GWL) in Eq. (5) and the groundwater potential ($\psi_{g,i}$) in Eq. (6), respectively.

$$RWU = RWU_s + RWU_g \quad (4)$$

$$RWU_s = \sum_{i=1}^{n} \frac{\psi_{s,i} - \psi_l}{r_{s,i} + r_{r,i} + r_{x,i}} \text{ for the soil layers above capillary fringe zone and above } d_{max} \quad (5)$$

$$RWU_g = \sum_{i=1}^{n} \frac{\psi_{g,i} - \psi_l}{r_{s,i} + r_{r,i} + r_{x,i}} \text{ for the soil layers below capillary fringe zone and above } d_{max} \quad (6)$$

For soil layers below d_{max}, RWU = RWU_g = 0

2.2. Study sites and data

The proposed model coupling was applied to 3 sites in the Netherlands covering both forest (Loobos) and meadow (Cabauw and VeenKampen) ecosystems (Fig. 2). The 3 sites have the typical temperate climate of the Netherlands, with an annual average precipitation of 700-900 mm yr^{-1} (Buishand et al., 2010; Brakkee et al., 2022), and air temperature of 10.5 °C (Bense & Kurylyk, 2017; Jansen et al., 2023). The Loobos site is located in the forested area of the Veluwe in the central part of the Netherlands, with an elevation of 25.0 m above sea level (a.s.l). The land cover is evergreen coniferous forest, and the soil type is loamy sandy soil (Heinen et al., 2021). The groundwater depth ranges from 3 to 4.5 m below land surface (Zhao et al., 2025; van der Molen et al., 2025). The Cabauw site is located in the central western region of the Netherlands, with an elevation of -0.7 m

https://doi.org/10.5194/egusphere-2025-4179
Preprint. Discussion started: 23 September 2025

below sea level. The land cover is grass, and the soil is a mixture of clay and peat (Heinen et al., 2021). The groundwater depth ranges from 0.0 to 1.25 m below land surface. The Veenkampen site is located in the Veluwe area in the central part of the Netherlands, with an elevation of 5.6 m a.s.l. The land cover is grass, and the soil is thin peat underlain by a clayey sand (Heinen et al., 2021). The groundwater depth ranges from 0.25 to 1 m below land surface.

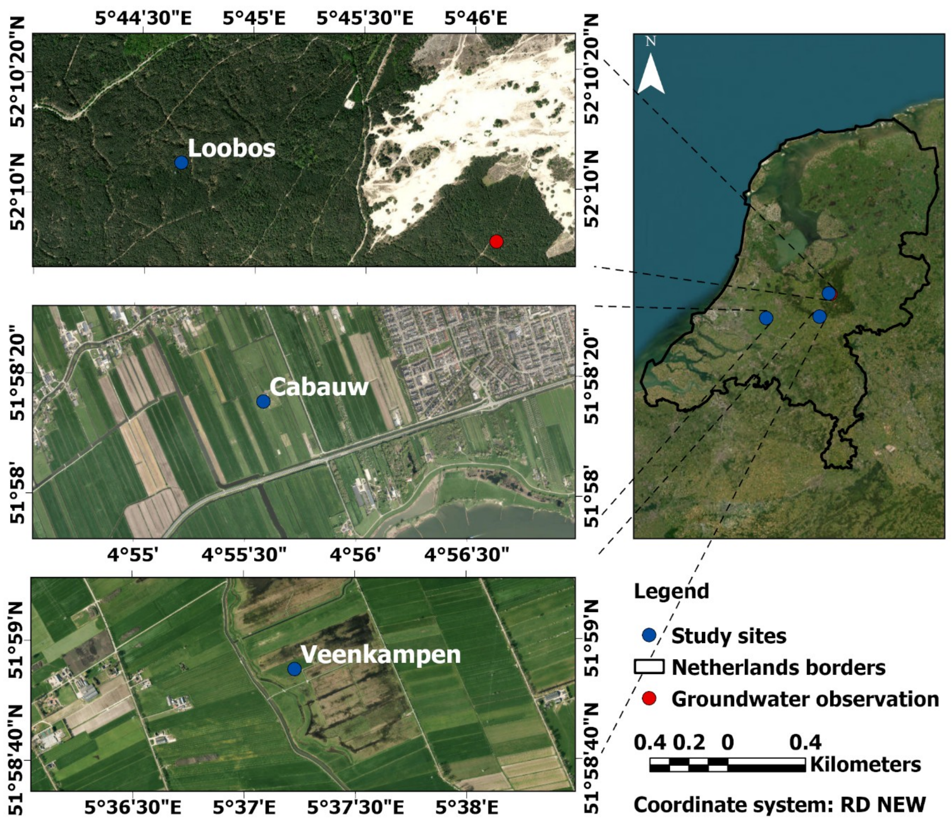

Figure 2. Location of the 3 study sites. Images are generated for the day 20 March 2025 using the ESRI ArcGIS Pro software

The forcing inputs and observations data for the 3 sites were collected from different sources (Table 2), and were processed to be compatible with the needed formats (Netcdf for STEMMUS-SCOPE and ASCII for MODFLOW 6). The forcing inputs include time series of the meteorological inputs (i.e.,

https://doi.org/10.5194/egusphere-2025-4179
Preprint. Discussion started: 23 September 2025

precipitation, net radiation, air temperature, wind speed, relative humidity, atmospheric pressure, and C02 dioxide concentration) and the leaf area index. The observation datasets, available for the entire simulation period, except for short gaps, at the 3 sites, were the profiles of θ and T_s, and ET. Other observation datasets were incomplete and include: a) the GPP, available only at the Loobos site for the period 2016-2021; b) the NEE, available only at the Cabauw site for the period 2016-2020; c) the GWL, not available exactly in the Loobos site, but retrieved from the nearest observation point about 500 m away (the red circle point in Fig. 2), assuming the same GWL; d) the GT, available only at the Loobos site for only one year (from 1 April 2023 to 31 March 2024); and e) the SIF data, available only at the Cabauw site on certain days in 2022 and 2023.

Table 2. Datasets acquisition at the 3 sites

Data	Loobos	Cabauw	Veenkampen
Meteorological inputs (precipitation, net radiation, air temperature, wind speed, relative humidity, atmospheric pressure and C02 dioxide concentration)	MAQ-dataset (van der Molen et al., 2024; 2025; Hong et al., 2025)	Cesar-dataset (Bosveld, 2020; KNMI, 2024)	MAQ-dataset (Heusinkveld et al., 2024)
Leaf area index	MODIS-LAI (Myneni et al., 2021)		
Observations (insitu measurements)			
Evapotranspiration, soil moisture, soil temperature	MAQ-dataset	Cesar-dataset	MAQ-dataset
Groundwater level	DINOloket (GDN, 2024)	Cesar-dataset	MAQ-dataset
Groundwater temperature	MAQ-dataset	Not available	Not available
Carbon fluxes (gross primary productivity and/or net ecosystem exchange)	MAQ-dataset	Cesar-dataset	Not available
Sun-induced chlorophyll fluorescence	Not available	(Colombo et al., 2024)	Not available

https://doi.org/10.5194/egusphere-2025-4179
Preprint. Discussion started: 23 September 2025

2.3. Models' setup

For brevity, from herein, the STEMMUS-SCOPE model is referred to as ST-SC and the STEMMUS-SCOPE-MODFLOW 6 model is referred to as ST-SC-MF6

2.3.1. Temporal and spatial discretization

Both ST-SC and ST-SC-MF6 models of the 3 sites used a 3 months model initialization phase (i.e., "spin-up") that extended from 1 January 2016 to 31 March 2016. After this, the simulation was run for a period of 8 years (from 1 April 2016 to 31 March 2024). The total simulation had 144,624 half-hourly time steps.

STEMMUS-SCOPE is a point-based model, while MODFLOW 6 is a grid-based model. As this study is the first example of coupling these two models, the ST-SC-MF6 models were set up in a vertically-stacked orientation (1-dimensional, 1D). The 1D models were assumed to be representative of the ecosystem of each of the corresponding sites.

The unsaturated zone in STEMMUS-SCOPE was modelled with site-specific total thicknesses: 5 m for Loobos, 1.5 m for Cabauw, and 1.2 m for Veenkampen – each exceeding the site's maximum observed water table depth (4.5 m for Loobos, 1.25 m for Cabauw, and 1 m for Veenkampen). The unsaturated zone was vertically discretized into 69, 50, and 33 layers for Loobos, Cabauw, and Veenkampen, respectively. The thickness of the layers was variable (minimum of 1 cm and maximum of 20 cm), started with finer resolution near the surface (1 cm), gradually increased to 20 cm, then gradually decreased again to 5 cm near the water table fluctuation zone.

The MODFLOW 6 models were horizontally discretized into a single cell that is 1 m by 1 m, and were vertically discretized into 20, 15, and 18 layers for the Loobos, Cabauw and Veenkampen sites, respectively. The layering information was retrieved from the BRO GeoTOP v1.6. geological model (TNO – GDN, 2023) and the BRO REGIS II v2.2.2. hydrogeological model (TNO – GDN, 2024). Since the

https://doi.org/10.5194/egusphere-2025-4179
Preprint. Discussion started: 23 September 2025

models were 1D models in the vertical direction, lateral flow considerations were neglected. To minimize the effect of this negligence, the saturated zone simulation was limited to the upper-most permeable hydrogeological unit, which terminates at a depth of 20 m below the land surface for Loobos and 9 m for both the Cabauw and Veenkampen sites. This permeable hydrogeological unit was then sub-divided into thinner layers, started with a thickness of 0.25 m, then smoothly increased to 0.5, 0.75, and 1 m. At the base of the bottom-most active layer, a specified flux boundary condition was applied to compensate for the neglected vertical flow from the excluded deeper hydrogeological units.

2.3.2. Initial and boundary conditions

Each model of the 3 sites was initialized by an initial θ and T_s for STEMMUS-SCOPE, and an initial GWL and GT for MODFLOW 6. The initial θ, T_s, GWL, and GT were retrieved from the collected datasets (Table 2) of the 3 sites as follows: a) 0.1, 5°C, 21.5 m, and 10°C for Loobos, b) 0.6, 5°C, -0.8 m and 10.5°C for Cabauw, and c) 0.75, 5°C, 5.1 m, and 11°C for Veenkampen.

The top boundary of the soil water module in STEMMUS-SCOPE was a specified flux (precipitation, input retrieved from the collected datasets in Table 2), and the bottom boundary was the GWL (received from MODFLOW 6). The top boundary of the soil energy module in STEMMUS-SCOPE was a specified temperature (air temperature, input retrieved from the collected datasets in Table 2), and the bottom boundary was the GT (received from MODFLOW 6). The top boundary of the GWF module of the saturated zone in MODFLOW 6 was the R_n (received from STEMMUS-SCOPE), and the bottom boundary was a specified flux (unknown value that was initially set to 0.0005 m day^{-1} and calibrated later). The top boundary of the GWE module of the saturated zone in MODFLOW 6 was the Q_{heat} and RT_g (received from STEMMUS-SCOPE), and the bottom boundary was a specified heat flux (unknown value that was initially set to 0.05 W m^{-2} and calibrated later).

https://doi.org/10.5194/egusphere-2025-4179
Preprint. Discussion started: 23 September 2025

2.3.3. Model parameters and calibration/validation

Both STEMMUS-SCOPE and MODFLOW 6 models have a lot of parameters – herein, only the parameters that had a high impact on the simulations (based on an earlier sensitivity analysis) are calibrated and listed in Table 3. The main parameters that govern the flow simulation in STEMMUS-SCOPE were: the vertical saturated hydraulic conductivity of the unsaturated zone (K_{sat}), residual water content (θ_r), saturated water content (θ_s), empirical coefficients of the Van Genuchten equation (α and n), and d_{max}. In MODFLOW 6, the main aquifer parameters were: the horizontal (K_h) and vertical (K_v) hydraulic conductivity, specific storage (S_s), and specific yield (S_y). While both STEMMUS-SCOPE and MODFLOW 6 used the same thermal parameters to simulate the heat transfer in both the unsaturated and the saturated zones, including: thermal conductivity of solids (K_T), specific heat capacity of solids (c_s), and bulk density (ρ_s). All the parameters in Table 3 were initialized with default values (not presented) and further calibrated.

The 8-year simulation period was divided into a 4-year calibration period (1 April 2016 to 31 March 2020), followed by a 4-year validation period (1 April 2020 to 31 March 2024). The collected observation datasets (Table 2) were used as calibration/validation state variables for the calibration/validation periods, respectively. The models were calibrated by trial and error until a satisfactory qualitative (graphical) and quantitative (statistical) match between the simulated variables and their observed equivalents was achieved. The goodness of fit was assessed using two statistical metrics: the Kling–Gupta efficiency (KGE; Gupta et al., 2009) and the root mean square error (RMSE). The KGE value can range from negative infinity to 1 and was deemed acceptable, when it was larger than zero (Knoben et al., 2019). The RMSE value was deemed acceptable, when it was minimized to 0.1 $m^3\ m^{-3}$, 2°C, 0.5 m, 1°C, 1 mm day^{-1}, 3 gC $m^{-2}\ day^{-1}$, 5 gC $m^{-2}\ day^{-1}$, and 0.25 mW $m^{-2}\ um^{-1}\ sr^{-1}$ for θ, T_s, GWL, GT, ET, GPP, NEE, and SIF, respectively.

https://doi.org/10.5194/egusphere-2025-4179
Preprint. Discussion started: 23 September 2025

429 Table 3. Models' tuned parameters

Parameter		Loobos	Cabauw	Veenkampen	Unit	Model
		Calibrated values				
K_{sat}	Vertical saturated hydraulic conductivity	2.5	20	20	cm day^{-1}	STEMMUS-SCOPE
θ_r	Residual water content	0.03	0.2	0.15	m^3 m^{-3}	STEMMUS-SCOPE
θ_s	Saturated water content	0.4	0.62	0.72	m^3 m^{-3}	STEMMUS-SCOPE
α	Alpha coefficient of Van Genuchten equation	0.1	0.09	0.02	cm^{-1}	STEMMUS-SCOPE
n	n coefficient of Van Genuchten equation	3.0	1.2	1.8	-	STEMMUS-SCOPE
d_{max}	Maximum rooting depth	400	50	50	cm	STEMMUS-SCOPE
K_h	Horizontal hydraulic conductivity	5.0	5.0	5.0	m day^{-1}	MODFLOW 6
K_v	Vertical hydraulic conductivity	5.0	5.0	5.0	m day^{-1}	MODFLOW 6
S_s	Specific storage	10^{-5}	$1.5*10^{-5}$	$1.5*10^{-5}$	-	MODFLOW 6
S_y	Specific yield	0.05	0.15	0.15	m^{-1}	MODFLOW 6
K_T	Thermal conductivity of solids	3.0	0.5	0.5	W m^{-1} $°C^{-1}$	Both models
c_s	Specific heat capacity of solids	3000	4000	4000	J kg^{-1} $°C^{-1}$	Both models
ρ_s	Bulk density of solids	1600	1600	1600	Kg m^{-3}	Both models

430 # 3. Results

431 ## 3.1. Loobos site

432 Figure 3 presents half-hourly observations and simulated outputs from the ST-SC and the ST-SC-MF6
433 models of the following: θ at depths 20, 50, and 100 cm (Figs. 3a, b, c); T_s at the same depths (Figs.
434 3d, e, f); GWL (Fig. 3g), and GT (Fig. 3h). The ST-SC-MF6 simulation of θ and T_s showed substantial
435 improvement over ST-SC, during both the calibration and the validation periods. The ST-SC
436 simulation showed an overestimation of the θ amplitude (fluctuations), which inversely affects

https://doi.org/10.5194/egusphere-2025-4179
Preprint. Discussion started: 23 September 2025

(dampens) the T_s amplitude, leading to lower T_s peaks and higher T_s troughs than the observations. In contrast, the ST-SC-MF6 simulation well captured the θ amplitude but overestimated the T_s amplitude, resulting in higher T_s peaks and lower T_s troughs than the observed T_s. The KGE values of θ at depths 20, 50, and 100 cm were 0.29, 0.46, 0.18 (Table 4) with corresponding RMSE values of 0.03, 0.02, 0.02 $m^3 m^{-3}$ (Table 5) for the ST-SC-MF6, as compared to KGE values equal to 0.02, 0.01, 0.02, and RMSE values equal to 0.05, 0.04, 0.04 $m^3 m^{-3}$ for the ST-SC, respectively. For T_s at the same depth, the ST-SC-MF6 yield KGE values of 0.49, 0.49, 0.56 (Table 4), with RMSE values of 1.73, 1.41, 1.72 °C (Table 5), as compared to KGE values equal to 0.42, 0.33, 0.22, and RMSE values equal to 2.39, 2.36, 2.73 °C for the ST-SC, respectively. Besides, the simulated GWL and GT by ST-SC-MF6 (Figs. 3g and h) showed a good match with the observations, with KGE values equal to 0.26 and 0.56 (Table 4), and RMSE values equal to 0.49 m and 0.17 °C (Table 5), respectively.

Table 4. KGE values of the state variables for the STEMMUS-SCOPE (ST-SC) and STEMMUS-SCOPE-MODFLOW 6 (ST-SC-MF6) models at the 3 sites over the entire period simulation

Variable		Loobos			Cabauw			Veenkampen	
		ST-SC	ST-SC-MF6		ST-SC	ST-SC-MF6		ST-SC	ST-SC-MF6
Θ at depth	20 cm	0.02	0.29	20 cm	0.29	0.7	7 cm	0.49	0.53
	50 cm	0.01	0.46	35 cm	0.37	0.57	13 cm	0.42	0.82
	100 cm	0.02	0.18	55 cm	0.49	0.55	25 cm	0.26	0.71
T_s at depth	20 cm	0.42	0.49	20 cm	0.85	0.84	10 cm	0.72	0.86
	50 cm	0.33	0.49	35 cm	0.76	0.67	20 cm	0.83	0.84
	100 cm	0.22	0.56	55 cm	0.64	0.78	50 cm	0.77	0.53
GWL		-	0.26		-	0.63		-	0.37
GT		-	0.56		-	-		-	-
ET		0.11	0.46		0.65	0.76		0.46	0.61
GPP		0.47	0.46		-	-		-	-

https://doi.org/10.5194/egusphere-2025-4179
Preprint. Discussion started: 23 September 2025

NEE	-	-	0.01	0.19	-	-
SIF	-	-	0.31	0.36	-	-

Table 5. RMSE values of the state variables for the STEMMUS-SCOPE (ST-SC) and STEMMUS-SCOPE-MODFLOW 6 (ST-SC-MF6) models at the 3 sites over the entire period simulation

Variable	Unit		Loobos			Cabauw			Veenkampen	
			ST-SC	ST-SC-MF6		ST-SC	ST-SC-MF6		ST-SC	ST-SC-MF6
θ at		20 cm	0.05	0.03	20 cm	0.14	0.08	7 cm	0.24	0.12
depth	$m^3\ m^{-3}$	50 cm	0.04	0.02	35 cm	0.17	0.1	13 cm	0.19	0.08
		100 cm	0.04	0.02	55 cm	0.18	0.08	25 cm	0.25	0.09
T_s at		20 cm	2.39	1.73	20 cm	1.2	1.6	10 cm	2.5	2.1
depth	°C	50 cm	2.36	1.41	35 cm	1.4	1.4	20 cm	2.2	2.2
		100 cm	2.73	1.72	55 cm	1.7	1.6	50 cm	2.9	2.5
GWL	m		-	0.49		-	0.21		-	0.26
GT	°C		-	0.17		-	-		-	-
ET	mm day^{-1}		1.37	0.99		0.95	0.76		1.12	0.87
GPP	gC $m^{-2}\ day^{-1}$		2.7	2.9		-	-		-	-
NEE	gC $m^{-2}\ day^{-1}$		-	-		7.0	4.6		-	-
SIF	mW $m^{-2}\ um^{-1}\ sr^{-1}$		-	-		0.21	0.28		-	-

Figure 4 illustrates daily observations and simulated evapotranspiration (ET) and gross primary productivity (GPP) from the ST-SC and ST-SC-MF6 models. The zoom windows in Figs. 4b, c, e, and f highlight the results during a dry period example in the calibration period (1 June 2019 – 30 September 2019) and in the validation period (1 June 2021 – 30 September 2021). The ST-SC-MF6 model exhibited a better match with the ET observations, particularly during the dry periods (Figs.

https://doi.org/10.5194/egusphere-2025-4179
Preprint. Discussion started: 23 September 2025

4b and c), as compared to ST-SC. The KGE and RMSE values were improved from 0.11 and 1.37 mm day^{-1} for ST-SC to 0.46 and 0.99 mm day^{-1} for ST-SC-MF6 (Table 4 and 5). Regarding GPP, both models aligned well with the observations during the simulation period, including the dry periods (Figs. 4e and f), with KGE and RMSE values equal to 0.46 and 2.9 gC m^{-2} day^{-1} for ST-SC-MF6, and equal to 0.47 and 2.7 gC m^{-2} day^{-1} for ST-SC, respectively (Table 4 and 5).

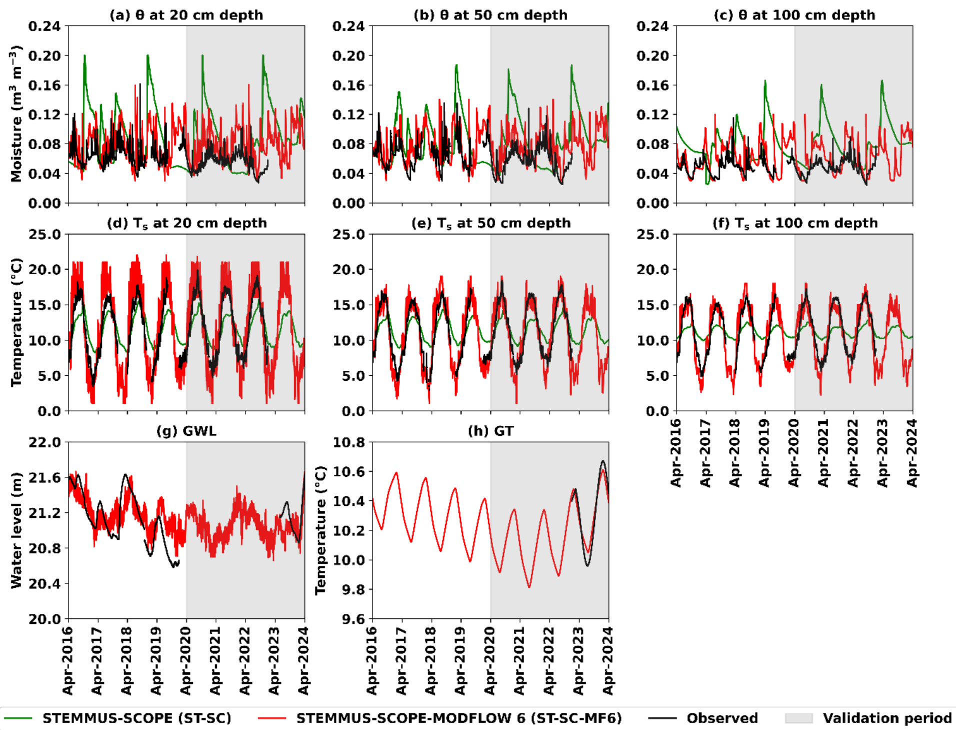

Figure 3. Loobos site – comparison of half-hourly simulated values by STEMMUS-SCOPE (green lines), by STEMMUS-SCOPE-MODFLOW 6 (red lines), and observed ones (black lines) during the calibration period (1 April 2016 – 31 March 2020) and the validation period (1 April 2020 – 31 March 2024; grey shaded) of the following: soil moisture (θ) at depths: a) 20 cm, b) 50 cm, c) 100 cm; soil temperature (T_s) at depths: d) 20 cm, e) 50 cm, f) 100 cm; g) groundwater level (GWL), and h) groundwater temperature (GT)

https://doi.org/10.5194/egusphere-2025-4179
Preprint. Discussion started: 23 September 2025

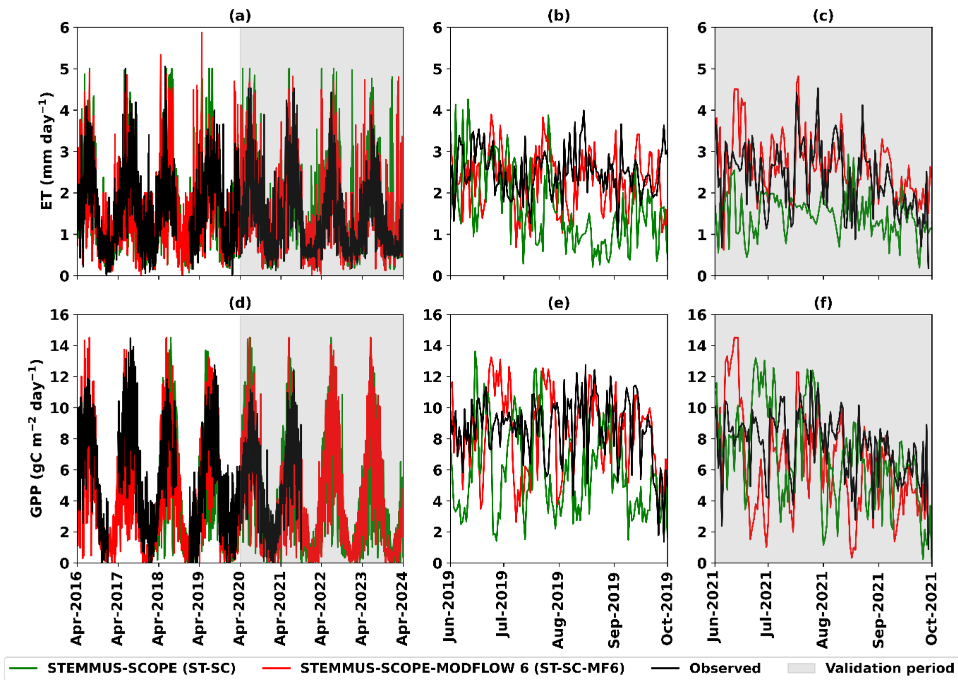

Figure 4. Loobos site – comparison of daily simulated values by STEMMUS-SCOPE (green lines), by STEMMUS-SCOPE-MODFLOW 6 (red lines), and observed ones (black lines) during the calibration period (1 April 2016 – 31 March 2020) and the validation period (1 April 2020 – 31 March 2024; grey shaded) of the following: a) evapotranspiration (ET) with two windows zooming in: b) a dry period example in the calibration period (1 June 2019 – 30 September 2019), c) a dry period example in the validation period (1 June 2021 – 30 September 2021); d) gross primary productivity (GPP) with two windows zooming in the same dry periods in: e) the calibration period, and f) the validation period

3.2. Cabauw site

Figure 5 presents half-hourly observations and simulated outputs from ST-SC and ST-SC-MF6 models of the following: θ at depths 20, 35, and 55 cm (Figs. 5a, b, c); T_s at the same depths (Figs. 5d, e, f); GWL (Fig. 5g), and GT (Fig. 5h). The ST-SC-MF6 simulation of θ demonstrated improved agreement with the observations during both the calibration and the validation periods, as compared to the ST-

https://doi.org/10.5194/egusphere-2025-4179
Preprint. Discussion started: 23 September 2025

SC simulation. The KGE values of θ at depths 20, 35, and 55 cm was improved to 0.7, 0.57, 0.55 for ST-SC-MF6, as compared to 0.29, 0.37, 0.49 for ST-SC, respectively (Table 4). The RMSE values of θ at the same depths were reduced to 0.08, 0.1, 0.08 m^3 m^{-3} for ST-SC-MF6, as compared to 0.14, 0.17, 0.18 m^3 m^{-3} for ST-SC, respectively (Table 5). Regarding T_s, both models generally correspond well with the observations except for the underestimated troughs by ST-SC-MF6 along the entire soil profile (Figs. 5d, e, and f). Both KGE and RMSE values of T_s at depths 20, 35, and 55 cm for both models were close to each other (Table 4 and 5). The KGE values were 0.84, 0.67, 0.78 for ST-SC-MF6 and 0.85, 0.76, 0.64 for ST-SC, respectively and the RMSE values were 1.6, 1.4, 1.6 °C for ST-SC-MF6 and 1.2, 1.4, 1.7 °C for ST-SC, respectively. Additionally, the ST-SC-MF6 simulated GWL showed a good match with the observations (Table 4 and 5), with KGE values equal to 0.63 and RMSE values equal to 0.21 m (Fig. 5g).

Figure 6 illustrates daily observations and simulated ET and NEE from ST-SC and ST-SC-MF6 models. The zoom windows in Figs. 6b, c, e, and f emphasize the results during a dry period example in the calibration period (1 June 2018 – 30 September 2018) and in the validation period (1 June 2020 – 30 September 2020). The ST-SC-MF6 model exhibited a closer agreement with the ET observations, particularly during the dry periods (Figs. 6b and c), as compared to ST-SC. The KGE and RMSE values were improved to 0.76 and 0.76 mm day^{-1} for ST-SC-MF6, as compared to 0.65 and 0.95 mm day^{-1} for ST-SC, respectively (Table 4 and 5). Similarly, for NEE, the ST-SC-MF6 model demonstrated a better match with the NEE observations, particularly during the dry periods (Figs. 6e and f), as compared to ST-SC. The KGE and RMSE values were improved to 0.19 and 4.46 gC m^{-2} day^{-1} for ST-SC-MF6, as compared to 0.01 and 7.0 gC m^{-2} day^{-1} for ST-SC, respectively (Table 4 and 5).

Figure 7 shows half-hourly observations and simulated SIF from ST-SC and ST-SC-MF6 on certain days, when the observed SIF data were available. During the summer days 9–14 August 2022 (Fig. 7a), the ST-SC-MF6 demonstrated an improved agreement with the SIF observations. Both models aligned well with the observations during days 3–6 June 2023 (Fig. 7c), which were dry days (Figs. 5a,

https://doi.org/10.5194/egusphere-2025-4179
Preprint. Discussion started: 23 September 2025

b, and c), while both models underestimate the SIF in the winter days 12–15 November 2022 (Fig. 7b). The ST-SC-MF6 showed slight improvement in the KGE and RMSE values of 0.36 and 0.21 mW m^{-2} um^{-1} sr^{-1}, as compared to 0.31 and 0.28 mW m^{-2} um^{-1} sr^{-1} for ST-SC, respectively (Table 4 and 5).

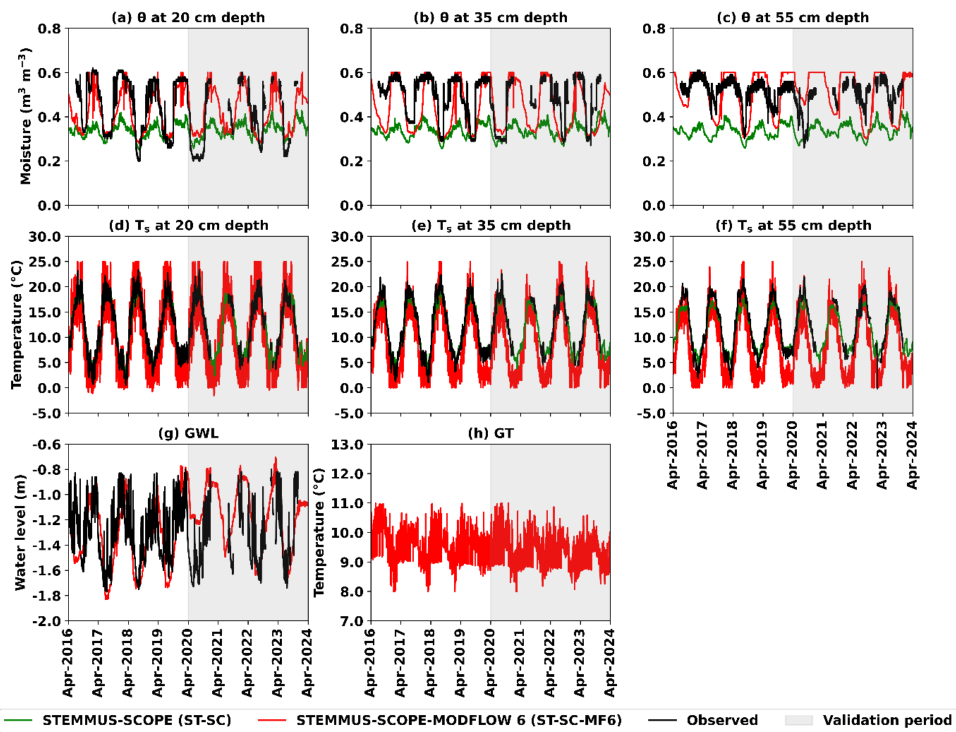

Figure 5. Cabauw site – comparison of half-hourly simulated values by STEMMUS-SCOPE (green lines), by STEMMUS-SCOPE-MODFLOW 6 (red lines), and observed ones (black lines) during the calibration period (1 April 2016 – 31 March 2020) and the validation period (1 April 2020 – 31 March 2024; grey shaded) of the following: soil moisture (θ) at depths: a) 20 cm, b) 50 cm, c) 100 cm; soil temperature (T_s) at depths: d) 20 cm, e) 50 cm, f) 100 cm; g) groundwater level (GWL), and h) groundwater temperature (GT)

https://doi.org/10.5194/egusphere-2025-4179
Preprint. Discussion started: 23 September 2025

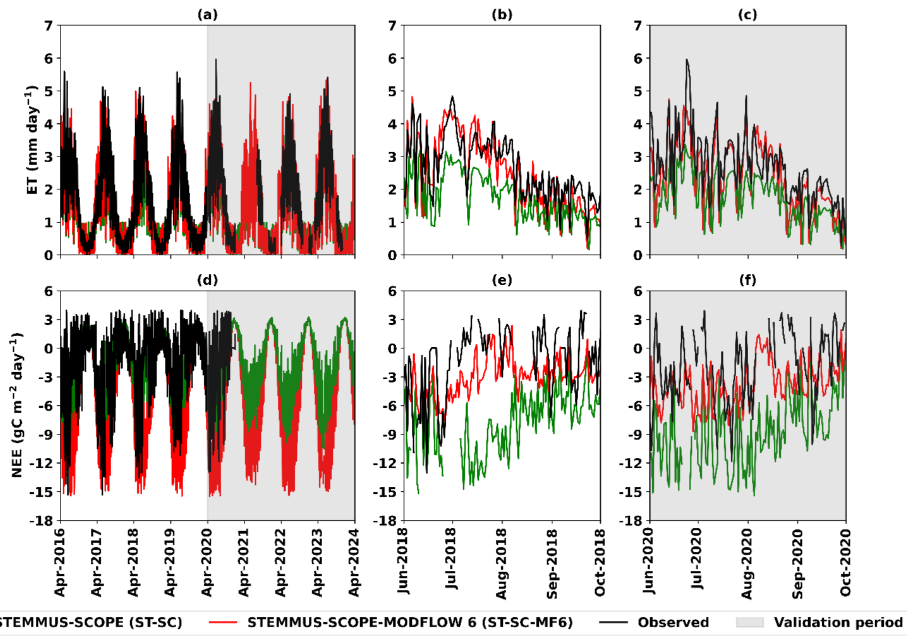

Figure 6. Cabauw site – comparison of daily simulated values by STEMMUS-SCOPE (green lines), by STEMMUS-SCOPE-MODFLOW 6 (red lines), and observed ones (black lines) during the calibration period (1 April 2016 – 31 March 2020) and the validation period (1 April 2020 – 31 March 2024; grey shaded) of the following: a) evapotranspiration (ET) with two windows zooming in: b) a dry period example in the calibration period (1 June 2018 – 30 September 2018), c) a dry period example in the validation period (1 June 2020 – 30 September 2020); d) net ecosystem exchange (NEE) with two windows zooming in the same dry periods in: e) the calibration period, and f) the validation period

https://doi.org/10.5194/egusphere-2025-4179
Preprint. Discussion started: 23 September 2025

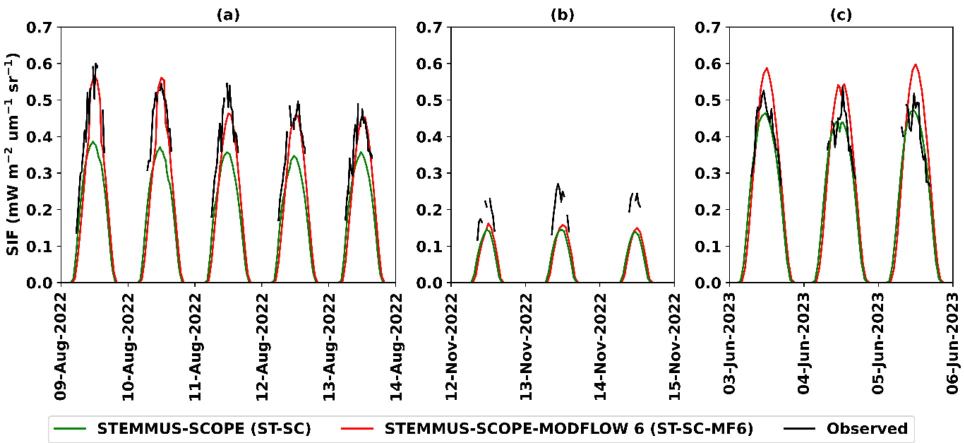

Figure 7. Cabauw site – comparison of half-hourly simulated sun-induced chlorophyll fluorescence (SIF) by STEMMUS-SCOPE (green lines), by STEMMUS-SCOPE-MODFLOW 6 (red lines), and observed ones (black lines) during the days: a) 9 August 2022 – 14 August 2022, b) 12 November 2022 – 15 November 2022, and c) 3 June 2023 – 6 June 2023

3.3. Veenkampen site

Figure 8 presents half-hourly observations and simulated outputs from ST-SC and ST-SC-MF6 models of the following: θ at depths 7, 13, and 25 cm (Figs. 8a, b, c); T_S at depths 10, 20, and 50 cm (Figs. 8d, e, f); GWL (Fig. g), and GT (Fig. 8h). The ST-SC-MF6 simulation of θ showed a better agreement with the observations during both the calibration and the validation periods, as compared to the ST-SC simulation (Figs. 8a, b, c). The KGE values of θ at depths 7, 13, and 25 cm were improved to 0.53, 0.82, and 0.71 for ST-SC-MF6, as compared to 0.49, 0.42, and 0.26 for ST-SC, respectively (Table 4). The RMSE values of θ at the same depths were reduced to 0.12, 0.08, 0.09 m^3 m^{-3} for ST-SC-MF6, as compared to 0.24, 0.19, 0.25 m^3 m^{-3} for ST-SC, respectively (Table 5). Regarding T_S, both models generally correspond well with the observations except for the overestimated peaks along the entire soil profile (Figs. 8d, e, and f). Both KGE and RMSE values of T_S at depths 10, 20, and 50 cm for both models were close to each other (Table 4 and 5). The KGE values were 0.86, 0.84, 0.53 for ST-SC-MF6 and 0.72, 0.83, 0.77 for ST-SC, respectively, and the RMSE values were 2.1, 2.2, 2.5 °C for ST-SC-MF6

https://doi.org/10.5194/egusphere-2025-4179
Preprint. Discussion started: 23 September 2025

and 2.5, 2.2, 2.9 °C for ST-SC, respectively. Additionally, the ST-SC-MF6 simulated GWL showed a good match with the observations (Table 4 and 5), with KGE values equal to 0.37, and RMSE values equal to 0.26 m (Fig. 8g).

Figure 9 illustrates daily observations and simulated ET from the ST-SC and ST-SC-MF6 models. The zoom windows in Figs. 9b and c highlight the results during a dry period example in the calibration period (June 2018 – September 2018) and in the validation period (June 2022 – September 2022). The ST-SC-MF6 model aligned more closely with the ET observations, particularly during the dry periods (Figs. 9b and c), as compared to ST-SC. The KGE and RMSE values of ET were improved to 0.61 and 0.87 mm d^{-1} for ST-SC-MF6, as compared to 0.46 and 1.12 mm d^{-1} for ST-SC, respectively (Table 4 and 5).

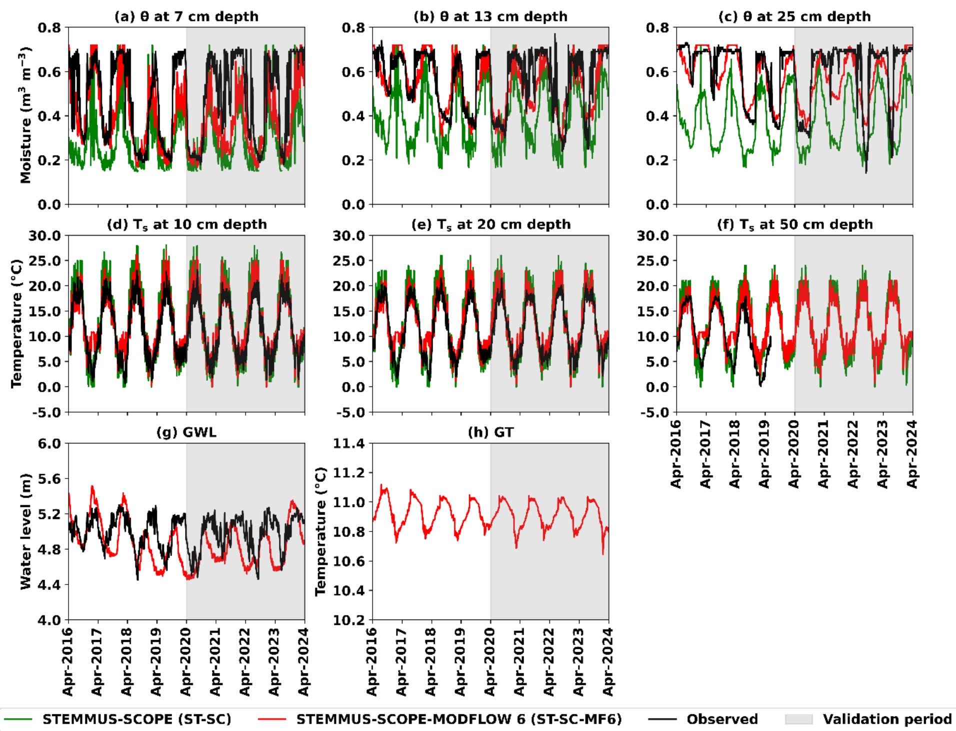

Figure 8. Veenkampen site – comparison of half-hourly simulated values by STEMMUS-SCOPE (green lines), by STEMMUS-SCOPE-MODFLOW 6 (red lines), and observed ones (black lines) during the

https://doi.org/10.5194/egusphere-2025-4179
Preprint. Discussion started: 23 September 2025

calibration period (1 April 2016 – 31 March 2020) and the validation period (1 April 2020 – 31 March 2024; grey shaded) of the following: soil moisture (θ) at depths: a) 20 cm, b) 50 cm, c) 100 cm; soil temperature (T_s) at depths: d) 20 cm, e) 50 cm, f) 100 cm; (g) groundwater level (GWL), and h) groundwater temperature (GT)

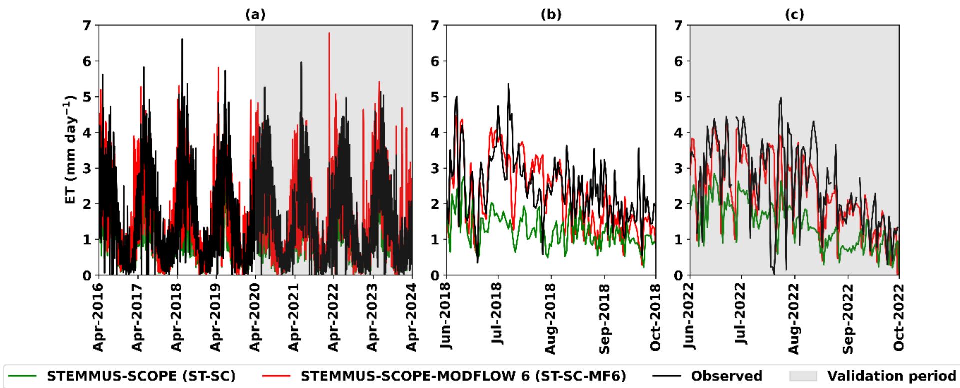

Figure 9. Veenkampen site – comparison of daily simulated evapotranspiration (ET) by STEMMUS-SCOPE (green lines), by STEMMUS-SCOPE-MODFLOW 6 (red lines), and observed ones (black lines) during the calibration period (1 April 2016 – 31 March 2020) and the validation period (1 April 2020 – 31 March 2024; grey shaded) with two windows zooming in: (b) a dry period example in the calibration period (1 June 2018 – 30 September 2018), and (c) a dry period example in the validation period (1 June 2022 –30 September 2022)

4. Discussion

The main objective of this study was to better understand what impact a more robust representation of groundwater has on modelling the soil-plant-atmosphere continuum. We hypothesized that explicitly representing groundwater mass and energy would improve modelling the soil-plant-atmosphere continuum. To achieve this, an IEM framework was developed by coupling the STEMMUS-SCOPE SPAC model to the MODFLOW 6 IHM. The coupling was implemented using

https://doi.org/10.5194/egusphere-2025-4179
Preprint. Discussion started: 23 September 2025

the BMI coupling approach (Peckham et al., 2013; Hutton et al., 2020). The BMI approach was followed because it facilitates the coupling at the shared interface between the respective models by exchanging the models' calculated variables through memory; thereby eliminating the need to modify the source code of either model. Hence, BMI allows for keeping up with advances of the individual models. Additionally, using BMI, the coupled models are run through executable files without the need to access the source code of the models during the models' simulation. Thus, BMI allows for coupling models that are written in different programming languages, as exemplified in this study (STEMMUS-SCOPE in MATLAB and MODFLOW 6 in Fortran).

The ST-SC-MF6 IEM was tested at 3 different sites (the Loobos forest, the Cabauw and Veenkampen meadow sites) in the Netherlands. Different key variables from the water, energy, and carbon cycles were analyzed for the two simulations (with and without coupling with MODFLOW 6) – namely, θ, T_s, GWL, GT, ET, GPP, NEE, and SIF. Comparing results (section 3) from the ST-SC and ST-SC-MF6 simulations highlights the benefits of representing the groundwater in models of soil-plant-atmosphere continuum.

4.1. Effect of groundwater on the soil profile

The GWL, simulated by MODFLOW 6, was used as a bottom boundary for the soil water module in STEMMUS-SCOPE; thereby influencing the $\psi_{s,i}$ and θ profiles. In the capillary fringe zone, above the GWL, soil is nearly saturated, causing the $\psi_{s,i}$ to become less negative, and the corresponding θ to increase significantly. Moving upward to the soil surface, the influence of the GWL gradually diminishes, and other surface forces (i.e. precipitation) become the dominant driver of $\psi_{s,i}$ and θ in the upper soil layers. However, the extent to which the GWL affects $\psi_{s,i}$ and θ depends on the thickness of the unsaturated zone where groundwater fluctuations occur. When the water table is shallow, its influence can extend upward beyond the lower soil layers, affecting the upper profile with decreasing intensity. Then, over time, as GWL rises, the entire $\psi_{s,i}$ profile shifts towards less negative and θ increases throughout the entire soil profile. Conversely, a falling GWL leads to a more

https://doi.org/10.5194/egusphere-2025-4179
Preprint. Discussion started: 23 September 2025

negative $\psi_{s,i}$ profile and a decrease in θ. In the Cabauw and Veenkampen sites, the groundwater depth is shallow (from 0 to 1.5 m below land surface); thus, the GWL had a significant impact on the θ profile. The GWL contribution is highlighted by a significantly improved match between the observed θ and the ST-SC-MF6 simulated one. By contrast, ST-SC underestimated the θ profile at the two sites (Figs. 5a, b, c and Fig. 8a, b, c). At the Loobos site, the GWL impact on the θ profile was not visible (Figs. 3a, b, c) because: 1) the Loobos site has a loamy sandy soil with a maximum observed θ along the entire profile roughly equal to 0.16 $m^3\ m^{-3}$, and potentially 2) the groundwater depth was relatively deep (3 to 4.5 m below land surface), as compared to the other two sites. However, confirming that the GWL impact on the θ profile is minor in cases where the groundwater depth ranges between 3 and 5 m needs further investigation. That could be done in the future by testing at different sites with similar groundwater depths (3 to 5 m) but different soil characteristics with generally higher θ than the Loobos site.

Similarly, the GT, simulated by MODFLOW 6, was used as a bottom boundary for the STEMMUS-SCOPE soil energy module. Using the calculated GT values improved the ST-SC simulation of the T_s profile for the Loobos site (Figs. 3d, e, and f). It is notable that matching the simulated T_s with the corresponding observations at the Loobos site was challenging. The Loobos site has low values of θ (maximum value = 0.16 $m^3\ m^{-3}$) along the soil profile, corresponding with relatively low T_s values (maximum value = 17.0 °C). Such a situation created extra difficulty to be modelled, since in STEMMUS-SCOPE, the θ and T_s are simulated together with many influencing factors as follows: 1) the low θ may shift the energy partitioning to more sensible heat and less latent heat, which leads to low values of evaporation and extra soil warming (overestimation of T_s profile), and 2) the thermal parameterization (thermal hydraulic conductivity and heat capacity) in STEMMUS-SCOPE follows the de Vries method (Yu et al., 2018), which is influenced by θ. In this case, the low θ values lowered the values of thermal parameters, which may lead to rapid soil heating and further contribute to the overestimation of T_s. Hence, the overestimation of the θ amplitude by ST-SC dampened the amplitude of the T_s. Conversely, the simulated θ by ST-SC-MF6 matched well the observations, but

https://doi.org/10.5194/egusphere-2025-4179
Preprint. Discussion started: 23 September 2025

the amplitude of the simulated T_s was slightly overestimated. The likely reason is the resistance scheme in the soil energy module in ST-SC, which follows the big leaf concept, assuming that the boundary layer resistance is the same for all canopy layers – a simplification that could be refined in the future. For the Cabauw and Veenkampen sites, the GT showed little impact on the T_s simulation (Figs. 5d, e, f, h, 8d, e, f and h) because there were no GT observations to control the simulation, and the values of temperature, used as bottom boundaries for the ST-SC and ST-SC-MF6 models, were similar.

4.2. Effect of groundwater on water fluxes

Incorporating the simulated GWL and GT by MODFLOW 6 as bottom boundaries in STEMMUS-SCOPE allowed for: 1) calculating the R_g, R_n and Cap fluxes (Eq. 2), and 2) proper simulation of the Q_{heat} and RT_g. The R_n, Q_{heat} and RT_g were then fed back into MODFLOW 6 to update the GWL and GT for the next time step. Allowing the two models to exchange simulated values contributed to a proper representation of the dynamics between the unsaturated and saturated zones and resulted in: i) a good match between the simulated and observed GWL (KGE = 0.26, 0.63, 0.37 and RMSE = 0.49, 0.21, 0.26 m, respectively) at the 3 sites (Figs. 3g, 5g, and 8g), ii) a good match between the simulated and observed GT (KGE = 0.56 and RMSE = 0.17 °C) at the Loobos site (Fig. 3h), iii) more accurate simulation of θ and T_s, and in so doing iv) improved the simulation of other variables such as ET, carbon fluxes (GPP and NEE), and SIF variables as discussed below.

The groundwater showed a significant impact on the simulated ET, which can be attributed to three reasons. First, the inclusion of GWL as a bottom boundary had improved the simulation of the soil matric potential ($\psi_{s,i}$) along the soil layers by proper seasonal dynamics of $\psi_{s,i}$ with respect to the position of the GWL. Consequently, RWU_s, which is based on $\psi_{s,i}$ (Eq. 5), was enhanced by 29.6 and 35.9% at the Cabauw and Veenkampen sites, respectively. Second, the capillary fringe zone (Fig. 1) was formed above the phreatic surface, where the Cap flux was calculated. The Cap flux further contributed to the water loss that moved upward to the ground surface, where E takes place

https://doi.org/10.5194/egusphere-2025-4179
Preprint. Discussion started: 23 September 2025

(Balugani et al., 2021; 2023). Additionally, the improvement in the simulated θ at the Cabauw and Veenkampen sites, together with the capillary fringe zone and Cap formation, enhanced the simulated E by 7.3 and 12.6%, respectively. Third, the $\psi_{g,i}$ was defined properly for the soil layers below the capillary fringe zone, which was further used to calculate RWU_g (Eq. 6). The RWU_g is an additional component that contributed by 17.0, 15.2, 13.0% to the total ET at the 3 sites (Loobos, Cabauw, and Veenkampen), respectively. The groundwater contribution to ET was more significant during dry periods (Figs. 4b, c, 6b, c, 8b, and c), when θ was depleted owing to lack of rains, while the GWL continued to support the water uptake by plant roots.

4.3. Effect of groundwater on carbon fluxes and SIF

Explicit representation of groundwater in the IEM also had an impact on the carbon fluxes (GPP and NEE), particularly during dry periods, even though groundwater is not explicitly represented in the carbon fluxes' calculations. Instead, θ, which is constrained by GWL, is included in the carbon fluxes' calculations and is positively correlated with carbon fluxes. When θ is limited (i.e., low water content), both $\psi_{s,i}$ and ψ_l decreased (became more negative), and the gradient between the $\psi_{s,i}$ and ψ_l shifted to more negative. With more negative ψ_l, the plant closed the stomata, so the stomatal conductance decreased in attempt to mitigate water stress. In contrast, higher θ increased the stomatal conductance, leading to higher CO2 uptake and higher GPP and NEE. Hence, NEE was increased at the Cabauw site (Figs. 6e and f) due to changes in simulated θ resulting from dynamically updated GWL values. Meanwhile, there was no effect on the simulated θ and consequently on the simulated GPP at the Loobos site (Fig. 4b and c) because the simulated GWL was deep (3 – 4.5 m) and maximum observed θ was generally low (0.16 $m^3 m^{-3}$).

Similarly, for the simulation of SIF, the impact of the groundwater system was evident at the Cabauw site through the changes in θ. The θ affects the water availability to the plant, which regulates the stomatal conductance and photosynthetic activity, and in turn contributes directly to the SIF calculations. The simulated SIF was enhanced in the dry summer days 9–14 August 2022 (Fig. 7a) due

https://doi.org/10.5194/egusphere-2025-4179
Preprint. Discussion started: 23 September 2025

to the enhanced θ, caused by shallow groundwater. Meanwhile, groundwater had no clear impact on the simulated θ during the summer days 3–6 June 2023 (Fig. 7c), since, during those days, both ST-SC and ST-SC-MF6 produced a very similar θ simulation (Figs. 5a, b, and c), resulting in no groundwater impact on the SIF simulation. While both models underestimated the SIF on the winter days 12–15 November 2022 (Fig. 7b), likely due to other parameters and/or forces that could influence the SIF calculations, which are beyond the scope of this study and need further investigation.

4.4. Recommendations

The changes in the θ, T_s, ET, GPP, NEE, and SIF variables suggest that accounting for groundwater interactions significantly improves the model's ability to represent the soil-plant-atmosphere continuum. However, certain assumptions and/or limitations highlight areas for future development. The coupling between STEMMUS-SCOPE and MODFLOW 6 was applied to three sites in the Netherlands, and only for 1D vertical flow. Future enhancements could include expanding the ST-SC-MF6 IEM to 2 or 3D scale and incorporating groundwater lateral flow and surface runoff. Moreover, the inconsistency in the amplitude of the simulated T_s (i.e., higher peaks or lower troughs than observations) could be addressed by improving the boundary layer resistance scheme in STEMMUS-SCOPE. Additionally, the incorporation of a more physically based simulation of SIF is expected to better capture the SIF dynamics, especially during winter periods.

5. Conclusion

This study demonstrated the added value of incorporating the groundwater component in modelling the soil-plant-atmosphere continuum. To achieve this, an IEM framework was developed by coupling the STEMMUS-SCOPE SPAC model with the MODFLOW 6 IHM, resulting in the ST-SC-MF6 IEM. The ST-SC-MF6 IEM was applied over an 8-year period (1 April 2016 – 31 March 2024) to 3 sites (Loobos,

https://doi.org/10.5194/egusphere-2025-4179
Preprint. Discussion started: 23 September 2025

Cabauw, Veenkampen) located in the Netherlands. Conditions varied across the three sites, including depth to groundwater, soil characteristics, vegetation, and water management (e.g. the GWL at Cabauw is managed and the surroundings of Veenkampen were converted into wetlands since 2020). The results supported the hypothesis that explicit groundwater representation enhances the quantification of the soil-plant-atmosphere continuum. Both qualitative and quantitative results highlighted the improved performance of the ST-SC-MF6, as compared to the ST-SC in representing soil-plant-atmosphere continuum. The groundwater contribution was found to be spatially (contrasting the 3 study sites) and temporally variable. The groundwater impact was more pronounced at the sites with a shallower water table (Cabauw and Veenkampen), as compared to the Loobos site. Additionally, the groundwater effects on the final IEM solution were more pronounced during dry periods, when shallow groundwater continued to support vegetation to mitigate water stress. Having demonstrated the utility of including groundwater in an IEM, the tool can be used to study the cause-and-effect relationships in the soil-plant-atmosphere continuum that may be increasingly important during dry periods that wear-on, leading to lower water tables. In this study, explicit representation of groundwater in the IEM facilitated the influence of groundwater on multiple soil and vegetation processes accomplished by: a) improving the simulation of the θ and T_s profiles, b) adding the RWU_g to the total ET, c) capturing the dynamics of the unsaturated and saturated zones by enabling dynamic exchange of the R_g, Cap, Q_{heat} fluxes and the GWL, GT, and RT_g variables between the two zones, and d) indirectly by refining the simulated θ and T_s profiles through better simulation of: i) the E and RWU_s, further both contribute to ET, ii) the carbon fluxes (GPP and NEE), and iii) the SIF. Overall, the findings of this study highlight the importance of the IEM framework for deepening the understanding of ecosystem functioning. Simply, including a more robust representation of groundwater in the ST-SC-MF6 IEM facilitated significant improvement in the simulated water, energy, and carbon cycles. Future work will address the current limitations (i.e., ignoring lateral groundwater flow and surface runoff, and simplifying the boundary layer resistance

https://doi.org/10.5194/egusphere-2025-4179
Preprint. Discussion started: 23 September 2025

scheme and SIF simulation) that were not resolved in this study and might further improve the accuracy and applicability of the ST-SC-MF6 IEM.

Code availability

STEMMUS-SCOPE v.1.6.1 is available as open-source code repository at https://github.com/EcoExtreML/STEMMUS_SCOPE. STEMMUS-SCOPE was run using the PyStemmusScope v0.5.0 Python package available at https://github.com/EcoExtreML/STEMMUS_SCOPE_Processing.

MODFLOW 6 v.6.6.0 is available at https://www.usgs.gov/software/modflow-6-usgs-modular-hydrologic-model and as open-source code repository from https://github.com/MODFLOW-ORG/modflow6. MODFLOW 6 was run using the modflowapi v0.3.0 Python package available at https://github.com/MODFLOW-ORG/modflowapi.

Authors contribution

Conceptualization: MGD, YZ, CVT, MWL, MSS, ZBS

Data curation: MGD, PK, HZ, MVM

Formal analysis: YZ, LY

Funding acquisition: YZ, CVT, ZBS

Methodology: All authors

Project administration: CVT

Software: MGD, FA, BS, ZS

https://doi.org/10.5194/egusphere-2025-4179
Preprint. Discussion started: 23 September 2025

Supervision: CVT, MWL, MSS

Visualization: MGD

Writing – original draft: MGD

Writing – review & editing: All authors

Competing interest

One of the co-authors (Zhongbo Su) is a member of the editorial board of the journal. Other authors declare that they have no conflict of interest.

Acknowledgements

The authors would like to acknowledge Guido Bakema from Wageningen Environmental Research for early discussions and David Berger and Mike from the U.S. Geological Survey for their review of the manuscript. We would also like to thank the Editor, the Associate Editor, and anonymous Reviewers for their constructive comments, which allowed us to improve the quality of the manuscript.

Any use of trade, firm, or product names is for descriptive purposes only and does not imply endorsement by the U.S. Government.

Financial support

This research was supported by the Faculty of Geo-Information Science and Earth Observation (ITC), University of Twente, the Netherlands. The authors would like to acknowledge the Netherlands

https://doi.org/10.5194/egusphere-2025-4179
Preprint. Discussion started: 23 September 2025

eScience Center **EcoExtreML** project (grant no. 27020G07), the Netherlands Organization for Scientific Research (NWO) KIC **WUNDER** project (grant no. KICH1. LWV02.20.004), and the European Union's Horizon Europe research and innovation programme **DRYAD** project (grant no. GA 101156076).

References

Akhter, T., Pokhrel, Y., Felfelani, F., Ducharne, A., Lo, M. H., & Reinecke, R. (2025). Implications of Lateral Groundwater Flow Across Varying Spatial Resolutions in Global Land Surface Modeling. Water Resources Research, 61(7), e2024WR038523. https://doi.org/10.1029/2024WR038523

Atkins, J. W., Bohrer, G., Fahey, R. T., Hardiman, B. S., Morin, T. H., Stovall, A. E. L., Zimmerman, N., & Gough, C. M. (2018). Quantifying vegetation and canopy structural complexity from terrestrial LiDAR data using the forestr r package. Methods in Ecology and Evolution, 9(10), 2057–2066. https://doi.org/10.1111/2041-210X.13061

Baatz, R., Hendricks Franssen, H. J., Euskirchen, E., Sihi, D., Dietze, M., Ciavatta, S., Fennel, K., Beck, H., De Lannoy, G., Pauwels, V. R. N., Raiho, A., Montzka, C., Williams, M., Mishra, U., Poppe, C., Zacharias, S., Lausch, A., Samaniego, L., Van Looy, K., … Vereecken, H. (2021). Reanalysis in Earth System Science: Toward Terrestrial Ecosystem Reanalysis. Reviews of Geophysics, 59(3), e2020RG000715. https://doi.org/10.1029/2020RG000715

Balugani, E., Lubczynski, M. W., & Metselaar, K. (2021). Evaporation Through a Dry Soil Layer: Column Experiments. Water Resources Research, 57(8), e2020WR028286. https://doi.org/10.1029/2020WR028286

Balugani, E., Lubczynski, M. W., Metselaar, K., & Balugani, E. (2023). Lysimeter and In-situ Field Experiments to Study Soil Evaporation through a Dry Soil Layer under Semi-Arid Climate. Water

https://doi.org/10.5194/egusphere-2025-4179
Preprint. Discussion started: 23 September 2025

Resources Research, e2022WR033878. https://doi.org/10.1029/2022WR033878

Balugani, E., Lubczynski, M. W., Reyes-Acosta, L., van der Tol, C., Francés, A. P., & Metselaar, K. (2017). Groundwater and unsaturated zone evaporation and transpiration in a semi-arid open woodland. Journal of Hydrology, 547, 54–66. https://doi.org/10.1016/J.JHYDROL.2017.01.042

Bense, V. F., & Kurylyk, B. L. (2017). Tracking the Subsurface Signal of Decadal Climate Warming to Quantify Vertical Groundwater Flow Rates. Geophysical Research Letters, 44(24), 12,244-12,253. https://doi.org/10.1002/2017GL076015

Benz, S. A., Irvine, D. J., Rau, G. C., Bayer, P., Menberg, K., Blum, P., Jamieson, R. C., Griebler, C., & Kurylyk, B. L. (2024). Global groundwater warming due to climate change. Nature Geoscience, 17(6), 545–551. https://doi.org/10.1038/s41561-024-01453-x

Bojinski, S., Verstraete, M., Peterson, T. C., Richter, C., Simmons, A., & Zemp, M. (2014). The Concept of Essential Climate Variables in Support of Climate Research, Applications, and Policy. Bulletin of the American Meteorological Society, 95(9), 1431–1443. https://doi.org/10.1175/BAMS-D-13-00047.1

Bosveld, F. C. (2020). The Cabauw In-situ Observational Program 2000 - Present: Instruments, Calibrations and Set-up. https://cdn.knmi.nl/knmi/pdf/bibliotheek/knmipubTR/TR384.pdf

Brakkee, E., Van Huijgevoort, M. H. J., & Bartholomeus, R. P. (2022). Improved understanding of regional groundwater drought development through time series modelling: The 2018-2019 drought in the Netherlands. Hydrology and Earth System Sciences, 26(3), 551–569. https://doi.org/10.5194/HESS-26-551-2022

Brunner, P., & Simmons, C. T. (2012). HydroGeoSphere: A Fully Integrated, Physically Based Hydrological Model. Ground Water, 50(2), 170–176. https://doi.org/10.1111/j.1745-6584.2011.00882.x

Buishand, A., Jilderda, R., & Wijngaard, J. (2010). KNMI - Regional differences in the extreme rainfall

https://doi.org/10.5194/egusphere-2025-4179
Preprint. Discussion started: 23 September 2025

climatology in the Netherlands. https://www.knmi.nl/kennis-en-datacentrum/achtergrond/regional-differences-in-the-extreme-rainfall-climatology-in-the-netherlands

Camporese, M., Paniconi, C., Putti, M., & Orlandini, S. (2010). Surface-subsurface flow modeling with path-based runoff routing, boundary condition-based coupling, and assimilation of multisource observation data. Water Resources Research, 46(2), 2512. https://doi.org/10.1029/2008WR007536

Chen, M., Xue, Y., Xue, Y., Peng, J., Guo, J., & Liang, H. (2024). Assessing the effects of climate and human activity on vegetation change in Northern China. Environmental Research, 247, 118233. https://doi.org/10.1016/J.ENVRES.2024.118233

Colombo, R., Julitta, T., Pacheco, J., Cogliati, S., Sabater, N., & van der Tol, C. (2024). Technical Assistance for the Development of Ground based Systems for Long term measurements of Red and Far red Sun Induced chlorophyll Fluorescence (DEFLOX) CCN4. https://www.jb-hyperspectral.com/research-field/

Cupertino, A., Dufour, S., & Rodríguez-González, P. M. (2024). Chasing success: A review of vegetation indicators used in riparian ecosystem restoration monitoring. Ecological Indicators, 166, 112371. https://doi.org/10.1016/J.ECOLIND.2024.112371

Dai, T., Dai, X., Lu, H., He, T., Li, W., Li, C., Huang, S., Huang, Y., Tong, C., Qu, G., Shan, Y., Liang, S., & Liu, D. (2024). The impact of climate change and human activities on the change in the net primary productivity of vegetation—taking Sichuan Province as an example. Environmental Science and Pollution Research, 31(5), 7514–7532. https://doi.org/10.1007/S11356-023-31520-6

Daoud, M. G., Lubczynski, M. W., Zoltan, V., & Francés, A. P. (2022). Application of a novel cascade-routing and reinfiltration concept with a Voronoi unstructured grid in MODFLOW 6, for an

https://doi.org/10.5194/egusphere-2025-4179
Preprint. Discussion started: 23 September 2025

assessment of surface-water/groundwater interactions in a hard-rock catchment (Sardon, Spain). Hydrogeology Journal, 1–27. https://doi.org/10.1007/S10040-021-02430-Z

Daoud, M. G., White, J. T., Morway, E. D., van der Tol, C., & Lubczynski, M. W. (2024). Remote sensing evapotranspiration in ensemble-based framework to enhance cascade routing and re-infiltration concept in integrated hydrological model applied to support decision making. Journal of Hydrology, 637, 131411. https://doi.org/10.1016/J.JHYDROL.2024.131411

de Conto, T., Armston, J., & Dubayah, R. (2024). Characterizing the structural complexity of the Earth's forests with spaceborne lidar. Nature Communications 2024 15:1, 15(1), 1–15. https://doi.org/10.1038/s41467-024-52468-2

de Wit, A., Boogaard, H., Fumagalli, D., Janssen, S., Knapen, R., van Kraalingen, D., Supit, I., van der Wijngaart, R., & van Diepen, K. (2019). 25 years of the WOFOST cropping systems model. Agricultural Systems, 168, 154–167. https://doi.org/10.1016/J.AGSY.2018.06.018

Dronova, I., & Taddeo, S. (2022). Remote sensing of phenology: Towards the comprehensive indicators of plant community dynamics from species to regional scales. Journal of Ecology, 110(7), 1460–1484. https://doi.org/10.1111/1365-2745.13897

Egidio, E., De Luca, D. A., & Lasagna, M. (2024). How groundwater temperature is affected by climate change: A systematic review. Heliyon, 10(6), 2405–8440. https://doi.org/10.1016/j.heliyon.2024.e27762

Elrashidy, M. T., Ireson, A. M., & Razavi, S. (2023). On the optimal level of complexity for the representation of groundwater-dependent wetland systems in land surface models. Hydrology and Earth System Sciences, 27(24), 4595–4608. https://doi.org/10.5194/HESS-27-4595-2023

Fatichi, S., Ivanov, V. Y., & Caporali, E. (2012). A mechanistic ecohydrological model to investigate complex interactions in cold and warm water-controlled environments: 1. Theoretical framework and plot-scale analysis. Journal of Advances in Modeling Earth Systems, 4(2), 5002.

https://doi.org/10.1029/2011MS000086

Gasper, F., Goergen, K., Shrestha, P., Sulis, M., Rihani, J., Geimer, M., & Kollet, S. (2014). Implementation and scaling of the fully coupled Terrestrial Systems Modeling Platform (TerrSysMP v1.0) in a massively parallel supercomputing environment - A case study on JUQUEEN (IBM Blue Gene/Q). Geoscientific Model Development, 7(5), 2531–2543. https://doi.org/10.5194/GMD-7-2531-2014

GCOS. (2025). Essential Climate Variables. Global Climate Observing System. https://gcos.wmo.int/site/global-climate-observing-system-gcos/essential-climate-variables

GDN. (2024). DINOloket - Data and Information of the Dutch Subsurface. Geological Survey of the Netherlands. https://www.dinoloket.nl/ondergrondgegevens

Golaz, J. C., Van Roekel, L. P., Zheng, X., Roberts, A. F., Wolfe, J. D., Lin, W., Bradley, A. M., Tang, Q., Maltrud, M. E., Forsyth, R. M., Zhang, C., Zhou, T., Zhang, K., Zender, C. S., Wu, M., Wang, H., Turner, A. K., Singh, B., Richter, J. H., … Bader, D. C. (2022). The DOE E3SM Model Version 2: Overview of the Physical Model and Initial Model Evaluation. Journal of Advances in Modeling Earth Systems, 14(12), e2022MS003156. https://doi.org/10.1029/2022MS003156;WGROUP:STRING:PUBLICATION

Graham, D. N., & Butts, M. B. (2005). FLEXIBLE INTEGRATED WATERSHED MODELING WITH MIKE SHE. In Watershed models, Eds. V. P. Singh & D. K. Frevert (pp. 245-272 Taylor and Francis). https://citeseerx.ist.psu.edu/document?repid=rep1&type=pdf&doi=4e9c3b289c52f7ff21471d7c3e9f357e66378ec9

Guo, Y. (1992). Simulation of water transport in the soil-plant-atmosphere system. https://doi.org/10.31274/RTD-180813-9473

Gupta, H. V., Kling, H., Yilmaz, K. K., & Martinez, G. F. (2009). Decomposition of the mean squared error and NSE performance criteria: Implications for improving hydrological modelling. Journal of Hydrology, 377(1–2), 80–91. https://doi.org/10.1016/J.JHYDROL.2009.08.003

Heinen, M., Brouwer, F., Teuling, C., & Walvoort, D. J. J. (2021). BOFEK2020 - Bodemfysische schematisatie van Nederland : update bodemfysische eenhedenkaart. Wageningen Environmental Research. https://doi.org/10.18174/541544

Heusinkveld, B. G., Barten, J. G. M., Fry, J. L., van der Molen, M., Nursanto, R. M., Ronda, R. J., & Snellen, H. (2024). MAQ-Observations v1.0: Veenkampen. https://maq-observations.nl/

Hughes, J. D., Langevin, C. D., & Banta, E. R. (2017). Documentation for the MODFLOW 6 framework. In U.S. Geological Survey Techniques and Methods 6-A57. https://doi.org/10.3133/tm6a57

Hughes, J. D., Russcher, M. J., Langevin, C. D., Morway, E. D., & McDonald, R. R. (2022). The MODFLOW Application Programming Interface for simulation control and software interoperability. Environmental Modelling & Software, 148, 105257. https://doi.org/10.1016/J.ENVSOFT.2021.105257

Hutton, E. W. h., Piper, M. D., & Tucker, G. E. (2020). The Basic Model Interface 2.0: A standard interface for coupling numerical models in the geosciences. Journal of Open Source Software, 5(51), 2317. https://doi.org/10.21105/JOSS.02317

Ireson, A. M., van der Kamp, G., Nachshon, U., & Butler, A. P. (2013). Modeling Groundwater-Soil-Plant-Atmosphere Exchanges in Fractured Porous Media. Procedia Environmental Sciences, 19, 321–330. https://doi.org/10.1016/J.PROENV.2013.06.037

Jansen, F. A., Jongen, H. J., Jacobs, C. M. J., Bosveld, F. C., Buzacott, A. J. V., Heusinkveld, B. G., Kruijt, B., van der Molen, M., Moors, E., Steeneveld, G. J., van der Tol, C., van der Velde, Y., Voortman, B., Uijlenhoet, R., & Teuling, A. J. (2023). Land Cover Control on the Drivers of Evaporation and Sensible Heat Fluxes: An Observation-Based Synthesis for the Netherlands. Water Resources Research, 59(11), e2022WR034361. https://doi.org/10.1029/2022WR034361

Kløve, B., Ala-Aho, P., Bertrand, G., Gurdak, J. J., Kupfersberger, H., Kværner, J., Muotka, T., Mykrä, H., Preda, E., Rossi, P., Uvo, C. B., Velasco, E., & Pulido-Velazquez, M. (2014). Climate change impacts on groundwater and dependent ecosystems. Journal of Hydrology, 518(PB), 250–266. https://doi.org/10.1016/J.JHYDROL.2013.06.037

KNMI. (2024). KNMI Data Platform. https://dataplatform.knmi.nl/organization/knmi

Knoben, W. J. M., Freer, J. E., & Woods, R. A. (2019). Technical note: Inherent benchmark or not? Comparing Nash-Sutcliffe and Kling-Gupta efficiency scores. Hydrology and Earth System Sciences, 23(10), 4323–4331. https://doi.org/10.5194/HESS-23-4323-2019

Langevin, C. D., Hughes, J. D., Banta, E. R., Niswonger, R. G., Panday, S., & Provost, A. M. (2017). Documentation for the MODFLOW 6 Groundwater Flow Model. In U.S. Geological Survey Techniques and Methods 6-A55. https://doi.org/10.3133/tm6a55

Langevin, C. D., Hughes, J. D., Provost, A. M., Russcher, M. J., & Panday, S. (2023). MODFLOW as a Configurable Multi-Model Hydrologic Simulator. Groundwater, 62(1), 111–123. https://doi.org/10.1111/GWAT.13351

Langevin, C. D., Provost, A. M., Panday, S., & Hughes, J. D. (2022). Documentation for the MODFLOW 6 Groundwater Transport Model. In U.S. Geological Survey Techniques and Methods 6-A61. https://doi.org/10.3133/TM6A61

Lawrence, D. M., Fisher, R. A., Koven, C. D., Oleson, K. W., Swenson, S. C., Bonan, G., Collier, N., Ghimire, B., van Kampenhout, L., Kennedy, D., Kluzek, E., Lawrence, P. J., Li, F., Li, H., Lombardozzi, D., Riley, W. J., Sacks, W. J., Shi, M., Vertenstein, M., … Zeng, X. (2019). The Community Land Model Version 5: Description of New Features, Benchmarking, and Impact of Forcing Uncertainty. Journal of Advances in Modeling Earth Systems, 11(12), 4245–4287. https://doi.org/10.1029/2018MS001583

Liao, C., Leung, L. R., Fang, Y., Tesfa, T., & Negron-Juarez, R. (2025). Representing lateral groundwater flow from land to river in Earth system models. Geoscientific Model

https://doi.org/10.5194/egusphere-2025-4179
Preprint. Discussion started: 23 September 2025

Development, 18(14), 4601–4624. https://doi.org/10.5194/GMD-18-4601-2025

Lubczynski, M. W., Leblanc, M., & Batelaan, O. (2024). Remote sensing and hydrogeophysics give a new impetus to integrated hydrological models: A review. Journal of Hydrology, 633, 130901. https://doi.org/10.1016/J.JHYDROL.2024.130901

Marchionni, V., Daly, E., Manoli, G., Tapper, N. J., Walker, J. P., & Fatichi, S. (2020). Groundwater Buffers Drought Effects and Climate Variability in Urban Reserves. Water Resources Research, 56(5), e2019WR026192. https://doi.org/10.1029/2019WR026192

Martínez-De La Torre, A., & Miguez-Macho, G. (2019). Groundwater influence on soil moisture memory and land-atmosphere fluxes in the Iberian Peninsula. Hydrology and Earth System Sciences, 23(12), 4909–4932. https://doi.org/10.5194/HESS-23-4909-2019

Milly, P. C. D. (1982). Moisture and heat transport in hysteretic, inhomogeneous porous media: A matric head-based formulation and a numerical model. Water Resources Research, 18(3), 489–498. https://doi.org/10.1029/WR018I003P00489

Morway, E. D., Provost, A. M., Langevin, C. D., Hughes, J. D., Russcher, M. J., Chen, C. Y., & Lin, Y. F. F. (2025). A New Groundwater Energy Transport Model for the MODFLOW Hydrologic Simulator. Groundwater. https://doi.org/10.1111/GWAT.13470

Muise, E. R., Andrew, M. E., Coops, N. C., Hermosilla, T., Burton, A. C., & Ban, S. S. (2024). Disentangling linkages between satellite-derived indicators of forest structure and productivity for ecosystem monitoring. Scientific Reports, 14(1), 1–15. https://doi.org/10.1038/s41598-024-64615-2

Myneni, R., Knyazikhin, Y., & Park, T. (2021). MODIS/Terra+Aqua Leaf Area Index/FPAR 4-Day L4 Global 500m SIN Grid V061 [Data set]. In NASA EOSDIS Land Processes DAAC. https://doi.org/10.5067/MODIS/MCD15A3H.061

Otoo, N. G., Sutanudjaja, E. H., van Vliet, M. T. H., Schipper, A. M., & Bierkens, M. F. P. (2025).

https://doi.org/10.5194/egusphere-2025-4179
Preprint. Discussion started: 23 September 2025

Mapping groundwater-dependent ecosystems using a high-resolution global groundwater model. Hydrology and Earth System Sciences, 29(8), 2153–2165. https://doi.org/10.5194/hess-29-2153-2025

Peckham, S. D., Hutton, E. W. H., & Norris, B. (2013). A component-based approach to integrated modeling in the geosciences: The design of CSDMS. Computers and Geosciences, 53, 3–12. https://doi.org/10.1016/j.cageo.2012.04.002

Rammler, M., & Bertermann, D. (2025). Groundwater temperatures downstream from a large-scale geothermal collector system (LSC) in Bad Nauheim, Germany. Grundwasser, 30(1), 37–48. https://doi.org/10.1007/s00767-024-00580-x

Ruehr, S., Girotto, M., Verfaillie, J. G., Baldocchi, D., Cabon, A., & Keenan, T. F. (2023). Ecosystem groundwater use enhances carbon assimilation and tree growth in a semi-arid Oak Savanna. Agricultural and Forest Meteorology, 342, 109725. https://doi.org/10.1016/J.AGRFORMET.2023.109725

Saccò, M., Mammola, S., Altermatt, F., Alther, R., Bolpagni, R., Brancelj, A., Brankovits, D., Fišer, C., Gerovasileiou, V., Griebler, C., Guareschi, S., Hose, G. C., Korbel, K., Lictevout, E., Malard, F., Martínez, A., Niemiller, M. L., Robertson, A., Tanalgo, K. C., … Reinecke, R. (2024). Groundwater is a hidden global keystone ecosystem. Global Change Biology, 30(1), e17066. https://doi.org/10.1111/GCB.17066

Samuel, J. B., & Chakraborty, A. (2023). Integration of a Groundwater Model to the Noah Land Surface Model for Aquifer-Soil Interaction. Journal of Advances in Modeling Earth Systems, 15(7), e2022MS003153. https://doi.org/10.1029/2022MS003153

Schilperoort, B. (2025). Sharing MATLAB models with everyone. Netherlands EScience Center. https://blog.esciencecenter.nl/sharing-matlab-models-with-everyone-499eaf0a2e9e

Senf, C. (2022). Seeing the System from Above: The Use and Potential of Remote Sensing for

Studying Ecosystem Dynamics. Ecosystems, 25(8), 1719–1737. https://doi.org/10.1007/S10021-022-00777-2

Shi, S., Yang, P., & van der Tol, C. (2023). Spatial-temporal dynamics of land surface phenology over Africa for the period of 1982–2015. Heliyon, 9(6), 16413. https://doi.org/10.1016/J.HELIYON.2023.E16413

Shrestha, P., Sulis, M., Masbou, M., Kollet, S., & Simmer, C. (2014). A Scale-Consistent Terrestrial Systems Modeling Platform Based on COSMO, CLM, and ParFlow. Monthly Weather Review, 142(9), 3466–3483. https://doi.org/10.1175/MWR-D-14-00029.1

Sun, Y., Gu, L., Wen, J., van der Tol, C., Porcar-Castell, A., Joiner, J., Chang, C. Y., Magney, T., Wang, L., Hu, L., Rascher, U., Zarco-Tejada, P., Barrett, C. B., Lai, J., Han, J., & Luo, Z. (2023). From remotely sensed solar-induced chlorophyll fluorescence to ecosystem structure, function, and service: Part I—Harnessing theory. Global Change Biology, 29(11), 2926–2952. https://doi.org/10.1111/GCB.16634

Tang, E., Zeng, Y., Wang, Y., Song, Z., Yu, D., Wu, H., Qiao, C., Van Der Tol, C., Du, L., & Su, Z. (2024). Understanding the effects of revegetated shrubs on fluxes of energy, water, and gross primary productivity in a desert steppe ecosystem using the STEMMUS-SCOPE model. Biogeosciences, 21(4), 893–909. https://doi.org/10.5194/BG-21-893-2024

TNO – GDN. (2023). BRO GeoTOP v1.6. TNO - Geological Survey of the Netherlands. https://www.dinoloket.nl/en/subsurface-models/map

TNO – GDN. (2024). BRO REGIS II v2.2.2. TNO - Geological Survey of the Netherlands. https://www.dinoloket.nl/en/subsurface-models/map

Van Cleemput, E., Adler, P. B., Suding, K. N., Rebelo, A. J., Poulter, B., & Dee, L. E. (2025). Scaling-up ecological understanding with remote sensing and causal inference. Trends in Ecology and Evolution, 40(2), 122–135. https://doi.org/10.1016/J.TREE.2024.09.006

https://doi.org/10.5194/egusphere-2025-4179
Preprint. Discussion started: 23 September 2025

van Dam, J. C., Groenendijk, P., Hendriks, R. F. A., & Kroes, J. G. (2008). Advances of Modeling Water Flow in Variably Saturated Soils with SWAP. Vadose Zone Journal, 7(2), 640–653. https://doi.org/10.2136/VZJ2007.0060

van der Molen, M., Barten, J. G. M., Snellen, H., Peters, W., & Vilà-Guerau de Arellano, J. (2024). MAQ-Observations v1.0: Loobos. https://maq-observations.nl/

Van Der Tol, C., Verhoef, W., Timmermans, J., Verhoef, A., & Su, Z. (2009). An integrated model of soil-canopy spectral radiances, photosynthesis, fluorescence, temperature and energy balance. Biogeosciences, 6(12), 3109–3129. https://doi.org/10.5194/BG-6-3109-2009

Van Walsum, P. E. V., & Supit, I. (2012). Influence of ecohydrologic feedbacks from simulated crop growth on integrated regional hydrologic simulations under climate scenarios. Hydrology and Earth System Sciences, 16(6), 1577–1593. https://doi.org/10.5194/HESS-16-1577-2012,

Wang, Y., Zeng, Y., Yu, L., Yang, P., Van Der Tol, C., Yu, Q., Lü, X., Cai, H., & Su, Z. (2021). Integrated modeling of canopy photosynthesis, fluorescence, and the transfer of energy, mass, and momentum in the soil-plant-Atmosphere continuum (STEMMUS-SCOPE v1.0.0). Geoscientific Model Development, 14(3), 1379–1407. https://doi.org/10.5194/GMD-14-1379-2021

Williams, M., Law, B. E., Anthoni, P. M., & Unsworth, M. H. (2001). Use of a simulation model and ecosystem flux data to examine carbon-water interactions in ponderosa pine. Tree Physiology, 21(5), 287–298. https://doi.org/10.1093/TREEPHYS/21.5.287

Williams, M., Rastetter, E. B., Fernandes, D. N., Goulden, M. L., Wofsy, S. C., Shaver, G. R., Melillo, J. M., Munger, J. W., Fan, S. M., & Nadelhoffer, K. J. (1996). Modelling the soil-plant-atmosphere continuum in a Quercus–Acer stand at Harvard Forest: the regulation of stomatal conductance by light, nitrogen and soil/plant hydraulic properties. Plant, Cell & Environment, 19(8), 911–927. https://doi.org/10.1111/J.1365-3040.1996.TB00456.X

Xin, P., Yu, X., Zhan, L., Cheng, H., & Yuan, S. (2023). Surface water-groundwater interaction affects

https://doi.org/10.5194/egusphere-2025-4179
Preprint. Discussion started: 23 September 2025

soil temperature distributions and variations in salt marshes. Advances in Water Resources, 172, 104366. https://doi.org/10.1016/J.ADVWATRES.2023.104366

Yang, X., Hu, J., Ma, R., & Sun, Z. (2021). Integrated Hydrologic Modelling of Groundwater-Surface Water Interactions in Cold Regions. Frontiers in Earth Science, 9. https://doi.org/10.3389/FEART.2021.721009

Yu, L., Zeng, Y., Wen, J., & Su, Z. (2018). Liquid-Vapor-Air Flow in the Frozen Soil. Journal of Geophysical Research: Atmospheres, 123(14), 7393–7415. https://doi.org/10.1029/2018JD028502

Zeng, J., Yang, J., Zha, Y., & Shi, L. (2019). Capturing soil-water and groundwater interactions with an iterative feedback coupling scheme: New HYDRUS package for MODFLOW. Hydrology and Earth System Sciences, 23(2), 637–655. https://doi.org/10.5194/HESS-23-637-2019

Zeng, Y., Alidoost, F., Schilperoort, B., Liu, Y., Verhoeven, S., Grootes, M. W., Wang, Y., Song, Z., Yu, D., Tang, E., Han, Q., Yu, L., Daoud, M. G., Khanal, P., Chen, Y., van der Tol, C., Zurita-Milla, R., Girgin, S., Retsios, B., … Su, Z. (2025). Towards an open soil-plant digital twin based on STEMMUS-SCOPE model following open science. Computers & Geosciences, 205, 106013. https://doi.org/10.1016/J.CAGEO.2025.106013

Zeng, Y., & Su, Z. (2013). STEMMUS : Simultaneous Transfer of Engery, Mass and Momentum in Unsaturated Soil. University of Twente, Faculty of Geo-Information Science and Earth Observation (ITC). https://research.utwente.nl/en/publications/stemmus-simultaneous-transfer-of-engery-mass-and-momentum-in-unsa

Zeng, Y., Su, Z., Barmpadimos, I., Perrels, A., Poli, P., Boersma, K. F., Frey, A., Ma, X., de Bruin, K., Goosen, H., John, V. O., Roebeling, R., Schulz, J., & Timmermans, W. (2019). Towards a Traceable Climate Service: Assessment of Quality and Usability of Essential Climate Variables. Remote Sensing, 11(10), 1186. https://doi.org/10.3390/RS11101186

https://doi.org/10.5194/egusphere-2025-4179
Preprint. Discussion started: 23 September 2025

Zeng, Y., Su, Z., Wan, L., & Wen, J. (2011a). A simulation analysis of the advective effect on evaporation using a two-phase heat and mass flow model. Water Resources Research, 47(10). https://doi.org/10.1029/2011WR010701

Zeng, Y., Su, Z., Wan, L., & Wen, J. (2011b). Numerical analysis of air-water-heat flow in unsaturated soil: Is it necessary to consider airflow in land surface models? Journal of Geophysical Research: Atmospheres, 116(D20), 20107. https://doi.org/10.1029/2011JD015835